AD-A084 185 GEORGIA INST OF TECH ATLANTA ENGINEERING EXPERIMENT --ETC F/G 20/3
STUDY OF SURFACE-PATCH TECHNIQUES FOR MODELING THREE-DIMENSIONA--ETC(U)
JAN 80 J J WANG F19628-78-C-0224

UNCLASSIFIED RADC -TR-79-337 NL

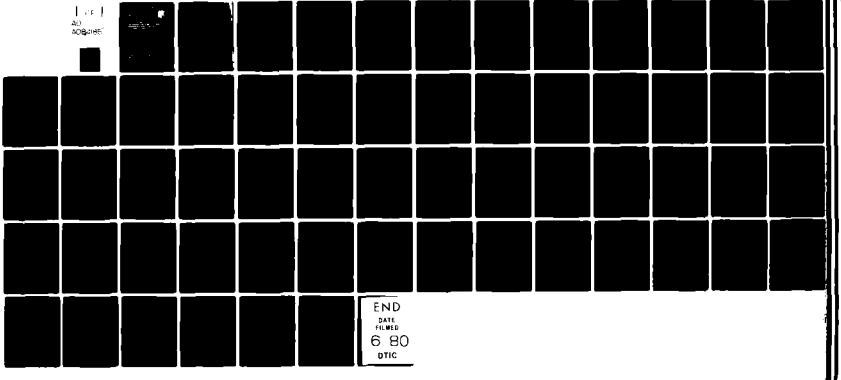

RADC-TR-79-337
Interim Report
January 1980

STUDY OF SURFACE-PATCH TECHNIQUES FOR MODELING THREE-DIMENSIONAL RADIATING OR SCATTERING OBJECTS

Georgia Institute of Technology

Johnson J. Wang

ROME AIR DEVELOPMENT CENTER
Air Force Systems Command
Griffiss Air Force Base, New York 13441

This report has been reviewed by the RADC Public Affairs Office (PA) and is releasable to the National Technical Information Service (NTIS). At NTIS it will be releasable to the general public including foreign nations.

RADC-TR-79-337 has been reviewed and is approved for publication.

APPROVED: Charles J. Drane

CHARLES J. DRANE
Contract Monitor

APPROVED: Allan C. Schell

ALLAN C. SCHELL, Chief
Electromagnetic Sciences Division

FOR THE COMMANDER: John P. Huss

JOHN P. HUSS
Acting Chief, Plans Office

If your address has changed or if you wish to be removed from the RADC mailing list, or if the addressee is no longer employed by your organization, please notify RADC (EEA), Hanscom AFB MA 01731. This will assist us in maintaining a current mailing list.

Do not return this copy. Retain or destroy.

(9) Interim rept. 15 Sep 78-15 Sep 79,

UNCLASSIFIED

SECURITY CLASSIFICATION OF THIS PAGE (When Data Entered)

(19) **REPORT DOCUMENTATION PAGE**

READ INSTRUCTIONS BEFORE COMPLETING FORM

1. REPORT NUMBER: RADC-TR-79-337 (14)	2. GOVT ACCESSION NO.: AD-A084185
3. RECIPIENT'S CATALOG NUMBER:	
4. TITLE (and Subtitle): STUDY OF SURFACE-PATCH TECHNIQUES FOR MODELING THREE-DIMENSIONAL RADIATING OR SCATTERING OBJECTS, (6)	5. TYPE OF REPORT & PERIOD COVERED: Interim Report September 78 - September 79
	6. PERFORMING ORG. REPORT NUMBER: N/A
7. AUTHOR(s): (10) Johnson J. Wang	8. CONTRACT OR GRANT NUMBER(s): F19628-78-C-0224 (5)
9. PERFORMING ORGANIZATION NAME AND ADDRESS: Georgia Institute of Technology, Engineering Experiment Station, Atlanta GA 30332 (16)	10. PROGRAM ELEMENT, PROJECT, TASK AREA & WORK UNIT NUMBERS: 61102F, 2305J326 (17) J3
11. CONTROLLING OFFICE NAME AND ADDRESS: Deputy for Electronic Technology (RADC/EEA), Hanscom AFB MA 01731 (11)	12. REPORT DATE: January 1980 (12) 60
	13. NUMBER OF PAGES: 55
14. MONITORING AGENCY NAME & ADDRESS (if different from Controlling Office): Same	15. SECURITY CLASS. (of this report): UNCLASSIFIED
	15a. DECLASSIFICATION/DOWNGRADING SCHEDULE: N/A

16. DISTRIBUTION STATEMENT (of this Report)

Approved for public release; distribution unlimited

17. DISTRIBUTION STATEMENT (of the abstract entered in Block 20, if different from Report)

Same

18. SUPPLEMENTARY NOTES

RADC Project Engineer: Charles J. Drane (EEA)

19. KEY WORDS (Continue on reverse side if necessary and identify by block number)

Method of Moments
Surface Patch Simulation
Electromagnetic Scattering and Radiation
Integral Equation Solution

20. ABSTRACT (Continue on reverse side if necessary and identify by block number)

A theoretical study of the surface patch technique for solving for the electromagnetic fields of three-dimensional scattering and radiating geometries was conducted. Improved techniques for the numerical calculations were also developed. In particular, the Georgia Tech surface-patch algorithm was improved and tested for conducting prolate spheroids, circular and rectangular cylinders, and cubes. The numerical results were good even for the finite cylinders with sharp edges. The merits of the surface-patch for solving the general three-dimensional electromagnetic problems have thus been demonstrated

DD FORM 1 JAN 73 1473 EDITION OF 1 NOV 65 IS OBSOLETE

153851

UNCLASSIFIED

SECURITY CLASSIFICATION OF THIS PAGE (When Data Entered)

The development of a new surface-patch algorithm for solving thinshell problems is also discussed in this report.

SUMMARY

The objective of this program is to investigate surface-patch modeling and to develop a user-oriented computer algorithm for analyzing general three-dimensional radiation and scattering problems with arbitrary surface geometries for airborne/ground-based applications. The existing surface-patch algorithm was improved and tested on prolate spheroids, circular and rectangular cylinders, and boxes. Good numerical results were obtained even for geometries with sharp edges. The merits of the surface-patch approach in solving electromagnetic problems of arbitrary geometries have been demonstrated for conducting bodies whose dimensions are not electrically large. Its advantages as well as disadvantages in comparison with the wire-grid approach were also discussed. Development of a new surface-patch algorithm was started with a reaction integral equation. This approach required intolerably large computer time in the integration process involved in the matrix computation. The electric field integral equation was then used to overcome this problem.

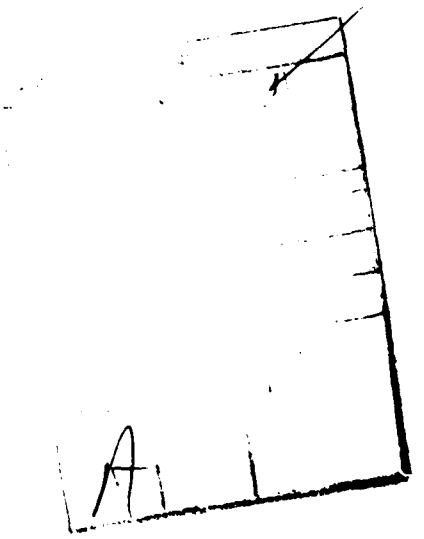

PREFACE

The research of this contract was carried out in the Electromagnetic Effectiveness Division of the Electronics Technology Laboratory of the Engineering Experiment Station at the Georgia Institute of Technology, Altanta, Georgia 30332. Dr. Johnson J. Wang served as the Project Director. This interim report covers the work which was performed from 15 September 1978 to 15 September 1979.

The author wishes to acknowledge the assistance of Mr. John Fay and Mr. Chris Papanicolopulos at Georgia Tech in the generation of numerical data and the exploration of the reaction integral equation. He also wishes to express thanks for fruitful and encouraging discussions with the technical monitor, Dr. Charles J. Drane.

TABLE OF CONTENTS

LIST OF FIGURES

LIST OF TABLES

SECTION I
INTRODUCTION

There are presently two types of approaches that have been employed to treat the scattering and radiation of arbitrarily-shaped conducting bodies that are not electrically large. The first is to simulate the conducting surface with thin wire grids and the second is to approximate the surface with patches. Research in the wire-grid approach has been very active, yet comparatively little effort has been devoted to the surface patch approach. Surface-patch modeling of arbitrarily-shaped bodies has been investigated by Oshiro, et al. [1,2], Albertsen, et al [3], and Wang [4].

The objectives of this research program are to investigate surface-patch modeling and to develop user-oriented computer programs for analyzing general three-dimensional radiation and scattering problems with arbitrary surface geometries for airborne and ground-based applications. The tasks include the evaluation and improvement of the existing Georgia Tech algorithm and the development of computer programs for thin-shell and antenna problems. This interim report summarizes the accomplishments during the first year of this two-year research program.

The algorithm improvement was primarily directed toward the reduction of execution time and the amount of central memory required in the numerical computation. Numerical testing was carried out for prolate spheroids, circular cylinders and rectangular cylinders (boxes) in order to determine the accuracy of the algorithm. Also, a computer program employing the electric field integral equation was developed to treat thin-shell problems which can not be computed using the existing Georgia Tech algorithm.

SECTION II

EVALUATION AND IMPROVEMENT OF EXISTING ALGORITHM

A. Basic Formulation

The existing computer program at Georgia Tech, as discussed in Reference 4, employs a magnetic field integral equation (MFIE) as follows

$$\underline{J}_s(\underline{r}) = \frac{1}{2\pi}\ \hat{n} \times \int \underline{J}_s(\underline{r}') \times \nabla'\phi\ (\underline{r},\underline{r}')ds'$$

$$= 2\hat{n} \times \underline{H}^{inc}(\underline{r}) \qquad \text{for } \underline{r} \in S\ , \tag{1}$$

where $\underline{J}_s$ = surface current density on the surface S,

$\hat{n}$ = an outward unit vector normal to S,

ϕ = $[\exp(-jk|\underline{r} - \underline{r}'|)]/|\underline{r} - \underline{r}'|$,

$\underline{r}$, $\underline{r}'$ = vectors from the origin to the field and source points,

$\underline{H}^{inc}$ = incident magnetic field intensity,

$\int$ = principal value integral, and

∇' = gradient operator with respect to the primed coordinates.

For the convenience of the present discussion, it is desirable to review the matrix generation process involved. We define the operator L as

$$L(\underline{J}_s(\underline{r})) = \underline{J}_s(\underline{r}) - \frac{1}{2\pi}\ \hat{n} \times \int_s \underline{J}_s(\underline{r}') \times \nabla'\phi ds'. \tag{2}$$

We now let

$$\underline{J}_s(\underline{r}) = \sum_{n=1}^{N} \underline{J}_n(\underline{r}), \tag{3}$$

and

$$\underline{J}_n(\underline{r}) = I_n^1 \underline{P}_n^1(\underline{r}) + I_n^2 \underline{P}_n^2(\underline{r}), \tag{4}$$

$$\underline{P}_n^i(\underline{r}) = \underline{U}_n^i \qquad \text{for } \underline{r}\epsilon\Delta S_n \tag{5}$$

$$\neq 0 \qquad \text{elsewhere,}$$

where $\underline{U}_n^1$ and $\underline{U}_n^2$ are orthonormal unit vectors on ΔS_n defined by

$$\underline{U}_n^1 = \frac{\hat{n} \times \underline{H}^{inc}(\underline{r})}{|\hat{n} \times \underline{H}^{inc}(\underline{r})|} \tag{6}$$

$$\underline{U}_n^2 = \hat{n}_n \times \underline{U}_n^1. \tag{7}$$

Using these relations, Equation (1) can be written in the form

$$L[\underline{P}_n^i(\underline{r})] = \underline{P}_n^i(\underline{r}) - \frac{1}{2\pi} \hat{n} \times \underline{U}_n^i \times \oint_{\Delta S_n} \nabla'\phi ds', \tag{8}$$

and we define the weighting function as

$$\underline{W}_m^i(\underline{r}) = \delta(\underline{r} - \underline{r}_m)\underline{P}_m^i(\underline{r}), \tag{9}$$

and the scalar product as

$$\langle P,Q \rangle = \int_S \underline{P} \cdot \underline{Q}\, ds. \tag{10}$$

Thus, by applying the weighting function to Equation (8), we have

$$\langle \underline{W}_m^i(\underline{r}), L[\underline{P}_n^i(\underline{r})] \rangle = \delta_m^n \cdot \delta_j^i - \frac{1}{2\pi} \underline{U}_m^i \cdot \hat{n}_m$$

$$\times \{\underline{U}_n^j \chi \oint_{\Delta s_n} \nabla' \phi(\underline{r}_m, \underline{r}') ds'\} \quad . \tag{11}$$

The magnetic field integral Equation (1) can be used to generate a system of linear equations by expanding the unknown surface current $\underline{J}_s$ according to Equation (3) and performing the scalar product according to Equation (11). The resulting system of linear equations can then be denoted by

$$\sum_{j=1}^{2} \sum_{n=1}^{N} I_n^j Z_{m\,n}^{i\,j} = V_m^i \tag{12}$$

$$m = 1,\ldots N$$
$$i = 1,2 \quad ,$$

where

$$Z_{m\,n}^{i\,j} = \langle \underline{W}_m^i(\underline{r}), L[\underline{P}_n^j(\underline{r})] \rangle$$

$$V_m^i = \langle \underline{W}_m^i(\underline{r}), 2\hat{n} \chi \underline{H}^{inc}(\underline{r}) \rangle \quad .$$

To solve for the unknown surface current I_n^i, one must first compute the matrix element Z_{mn}^{ij} which involves an integration process according to Equation (11). The existing Georgia Tech computer algorithm is based upon the formulation which is summarized in the preceding equations. The methods of evaluation of the matrix elements and matrix solution, together with the techniques which have been developed to improve the computer algoirthm will be discussed in the following paragraphs.

B. Matrix Symmetry

Execution time and central memory size are primary considerations in the present analysis. It is desirable to explore the possibility of

attaining a symmetrical property for the square matrix Z_{mn}^{ij}. A symmetrical matrix requires only about half the execution time and central memory as does an unsymmetrical matrix. Thus, symmetry will make it possible to compute the EM field for scattering and radiating bodies of larger size.

The square matrix Z_{mn}^{ij} can be arranged in the following form

$$[Z_{m\,n}^{i\,j}] = \begin{Bmatrix} [Z_{m\,n}^{1\,1}] & [Z_{m\,n}^{1\,2}] \\ [Z_{m\,n}^{2\,1}] & [Z_{m\,n}^{2\,2}] \end{Bmatrix} , \tag{13}$$

which consists of four sub-matrices each of which has a NxN dimension.

Letting

$$\kappa = m + (i-1)N, \tag{14}$$

$$\ell = n + (j-1)N, \tag{15}$$

we have

$$C_{\ell}^{\kappa} = Z_{m\,n}^{i\,j} . \tag{16}$$

For $[Z_{mn}^{ij}]$ to be symmetrical, it is necessary, by definition, that

$$C_{\ell}^{\kappa} = C_{\kappa}^{\ell} , \tag{17}$$

or

$$\begin{aligned} Z_{m\,n}^{i\,j} &= C_{\ell}^{\kappa} = C_{\kappa}^{\ell} \\ &= Z_{n\,m}^{j\,i} . \end{aligned} \tag{18}$$

Substitution of Equation (11) into Equation (18) yields

$$\underline{U}_m^i \cdot \hat{n}_m \times \{\underline{U}_n^j \times \oint_{\Delta S_n} \nabla'\phi\ (\underline{r}_m, \underline{r}')ds'\}$$

$$= \underline{U}_n^i \cdot \hat{n}_n \times \{\underline{U}_m^j \times \oint_{\Delta S_m} \nabla'\phi\ (\underline{r}_n, \underline{r}')ds'\} \tag{19}$$

which is the condition for a symmetrical matrix $[Z_{mn}^{ij}]$. In general, Equation (19) can not be satisfied and therefore symmetry for the matrix can not be readily achieved.

Galerkin's method, which chooses identical sets of basis and weighting functions, is more likely to yield symmetrical matrices. In the present case, this can be explored by selecting equal patch sizes and weighting functions as follows

$$\underline{W}_m^i(\underline{r}) = \underline{P}_m^i(\underline{r}). \tag{20}$$

The condition for matrix symmetry in this case is

$$\underline{U}_m^i \cdot \hat{n}_m \times \{\underline{U}_n^j \times \int_{\Delta S_m} \oint_{\Delta S_n} \nabla'\phi(\underline{r}, \underline{r}')ds'ds\}$$

$$= \underline{U}_n^j \cdot \hat{n}_n \times \{\underline{U}_m^i \times \int_{\Delta S_n} \oint_{\Delta S_m} \nabla'\phi(\underline{r}, \underline{r}')ds'ds\}, \tag{21}$$

which can be reduced to

$$\underline{U}_m^i \cdot \hat{n}_m \times \underline{U}_n^j = \underline{U}_n^j \cdot \hat{n}_n \times \underline{U}_m^i \quad , \tag{22}$$

or

$$\underline{U}_n^j \cdot \underline{U}_m^{1+\delta_1^i} (-1)^j = \underline{U}_m^i \cdot \underline{U}_n^{1+\delta_1^j} (-1)^i \tag{23}$$

Unfortunately, Equation (23) can not be satisfied on a general three-dimensional surface. If we let

$$I_n^2 = 0 \quad \text{for } n = 1, \ldots N \tag{24}$$

in Equation (4), Equation (23) is reduced to

$$\underline{U}_n^1 \cdot \underline{U}_m^2 = \underline{U}_m^1 \cdot \underline{U}_n^2 \ . \tag{25}$$

This is similar to wire-grid modeling, in which the direction of the current is along the pre-determined wire structure. The condition stated by Equation (25) is still too restrictive to be satisfied on a general closed surface.

The above discussion can also be reviewed on the basis of linear algebra, which attributes the symmetry of the matrix to the self-conjugate property of the linear operator L [5]. As long as one selects an orthonormal basis for a space, then self-conjugate operators are in a natural one-to-one correspondence with symmetrical matrices. The difficulty in attaining matrix symmetry therefore appears to be due to the magnetic field integral equation for which the operator L is not self-conjugate. It is therefore necessary to modify the operator L , or the magnetic field integral equations, before a further step to attain matrix symmetry is attempted.

In the wire scattering and radiation analysis, apparently the only algorithm having a symmetrical matrix is the reaction integral equation developed by Richmond [6]. The original operator was not self-conjugate and the matrix therefore asymmetric. However, by approximating the

surface integral over the tubular expansion dipole with a line integral, the matrix element, or the mutual impedance between two dipoles, was made symmetrical. Other computer programs do not have a symmetrical matrix in their computation. However, matrix reduction for geometrically symmetrical scatterers and radiators has been recognized and practiced such as in the WAMP program [7], the work by Sancer, et al. [8], and Tsai, et al. [9]. In the present algorithm, matrix reduction for a symmetrical scatterer was implemented and will be discussed next in this section.

C. Symmetrical Scatterers

When the direction of propagation of an incident plane wave is in the plane of symmetry of a conducting scatterer, it is recognized that some symmetric behavior must exist in the induced current on the surface of the scatterer. This property has been taken advantage of by various authors in their effort to reduce the central memory size required in the computer run [7-9].

Without loss of generality, Cartesian coordinates can be set up so that the plane of symmetry coincides with the XZ plane as shown in Figure 1. The polarization of the incident wave is assumed to be either parallel or perpendicular to the XZ plane. Arbitrary polarizations can be decomposed into two components, one parallel and the other perpendicular to the XZ plane. The overall scattering problem can then be treated by superposing the fields due to these two component incident fields.

At two symmetrical points I and I+N/2 in Figure 1, the components of the induced surface currents exhibit the following relationships

$$
\begin{aligned}
J_I^{1x} &= J_{I+N/2}^{1x} \quad , \\
J_I^{1y} &= -J_{I+N/2}^{1y} \quad , \\
J_I^{1z} &= J_{I+N/2}^{1z} \quad , \\
J_I^{2x} &= -J_{I+N/2}^{2x} \quad , \\
J_I^{2y} &= J_{I+N/2}^{2y} \quad , \\
J_I^{2z} &= -J_{I+N/2}^{2z} \quad ,
\end{aligned}
\tag{26}
$$

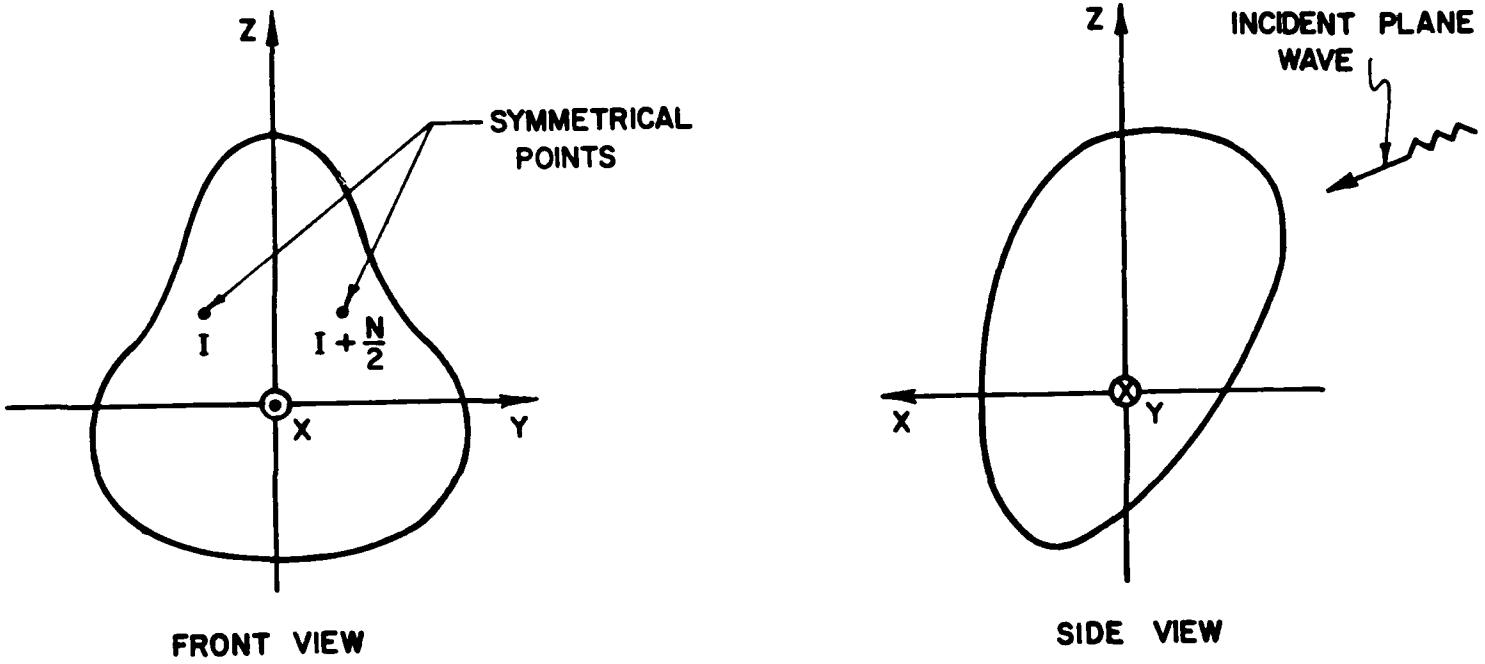

PLANE OF SYMMETRY - XZ

Figure 1. A symmetrical scatterer illuminated by a plane wave incident in the plane of symmetry.

when $\underline{H}_1$ is perpendicular to the plane of symmetry (XZ plane). In Equation (26), J^{ix} denotes, for example, the x component of $I_I^1 \underline{P}_n^1$ in Equation (4).

When $\underline{H}_1$ is parallel to the plane of symmetry, the induced current on the scatterer has the following property

$$
\begin{aligned}
J_I^{1x} &= -J_{I+N/2}^{1x} \quad , \\
J_I^{1y} &= J_{I+N/2}^{1y} \quad , \\
J_I^{1z} &= -J_{I+N/2}^{1z} \quad , \\
J_I^{2x} &= J_{I+N/2}^{2x} \quad , \\
J_I^{2y} &= -J_{I+N/2}^{2y} \quad , \\
J_I^{2z} &= J_{I+N/2}^{2z} \quad .
\end{aligned}
\tag{27}
$$

Equations (26) and (27) show that the number of unknowns in Equation (12) can be reduced from a total of 2N to N. This can be carried out by the following reduction process

$$
\begin{aligned}
\sum_{n=1}^{N} \sum_{j=1}^{2} I_n^j Z_{mn}^{ij} &= \sum_{n=1}^{N/2} \sum_{j=1}^{2} I_n^j Z_{mn}^{ij} + \sum_{n=N/2+1}^{N} \sum_{j=1}^{2} I_n^j Z_{mn}^{ij} \\
&= \sum_{n=1}^{N/2} \sum_{j=1}^{2} I_n^j \left[Z_{mn}^{ij} + Z'^{ij}_{m(n+N/2)} \right] ,
\end{aligned}
\tag{28}
$$

where
$$
Z'^{ij}_{m(n+N/2)} = \langle \underline{W}_m^i (\underline{r}), L[\underline{\underline{C}}_{Ip}^j \cdot \underline{P}_n^j (\underline{r})] \rangle , \tag{29}
$$

where $\underline{\underline{C}}_{Ip}^j$ is a dyad defined as

$$\underline{\underline{C}}^{j}_{Ip} = (-1)^{(j-1)}\{(-1)^{Ip+j+1}\hat{x}\hat{x} + (-1)^{Ip+j+2}\hat{y}\hat{y} + (-1)^{Ip+j+3}\hat{z}\hat{z}\} \tag{30}$$

Ip = 1 if $\underline{H}^i$ // x-z plane

= 2 if $\underline{H}^i \perp$ x-z plane

Equation (12) can now be written as

$$\sum_{n=1}^{N/2}\sum_{j=1}^{2} I_n^j \left[Z_{mn}^{ij} + Z'^{ij}_{m(n+N/2)}\right] = V_m^i \qquad \begin{matrix} i = 1,2 \\ m = 1,\ldots N/2 \end{matrix} \tag{31}$$

The total number of equations is then reduced to one half of the original number and the matrix size to one fourth of the original size.

D. Matrix Computation

The matrix element Z_{mn}^{ij}, according to Equations (11) and (12), involves an integral of the following form

$$\underline{I}_n^m = \int_{\Delta S_n} \nabla'\phi\ (\underline{r}_m, \underline{r}')\ ds'. \tag{32}$$

Computation of the integral $\underline{I}_n^m$ is very time consuming if carried out numerically. However, it has been observed that

$$\underline{I}_n^m \sim \nabla'\phi\ (\underline{r}_m, \underline{r}_n)\ \Delta S_n, \tag{33}$$

where $\underline{r}_n$ is the position vector to the center of the nth patch and ΔS_n is its area. The approximation in Equation (33) improves as the shape of the nth patch approaches an equiangular triangle.

Figure 2 shows, without loss of generality, the nth triangular patch coincidng with the X'-Y' plane, one vertex on Y' axis, and the opposite side on X' axis. The integrand can be simplified by the following approximation

$$\phi\ (\underline{r}_m,\ \underline{r}') \sim e^{-jkR_{mn}}\ [1-jk\ (R-R_{mn})]/R, \tag{34}$$

which is a two-term Taylor expansion of e^{-jkr} in the neighborhood of R_{mn}, where $R = |\underline{r}_m - \underline{r}'|$, $R_{mn} = |\underline{r}_m - \underline{r}_n|$ as in Figure 3. The validity of Equation (34) depends on the following condition

$$k\ |R-R_{mn}| \ll 1. \tag{35}$$

Since the patch size is limited to, say, $\lambda/3$ or less on each side of the triangle, it is generally true that

$$k\ |R-R_{mn}| < 1. \tag{36}$$

It can be shown that the self patch integral $\underline{I}_n^{\ n}$ vanishes when the patch is equilateral and small enough to satisfy Equation (35). Therefore

$$\underline{I}_n^{\ n} \tilde{=} 0 \tag{37}$$

In proving Equation (37), it was noted that Equation (35) was well satisfied in the immediate vicinity of R_{mn}, where $|R - R_{nm}| \sim |R| \sim 0$.

When $m \neq n$, two separate patches are involved, the integral $\underline{I}_n^{\ m}$ becomes considerably more complicated but can be approximated in closed form as follows

$$\underline{I}_n^{\ m} \sim (1 + jkR_{mn})\ e^{-jkR_{mn}}\ \{\hat{x}'I_x + \hat{y}'I_y\},$$

where

$$I_x = \frac{1}{\sqrt{1 + \left(\frac{x_2'}{y_1'}\right)^2}} \ln\left\{\left[(x-x_2')^2 + y^2 + z^2 + \left(\frac{2x_2'}{y_1'}(x-x_2') - 2y\right) y_1'\right.\right.$$

$$\left.\left. + \left(\left(\frac{x_2'}{y_1'}\right)^2 + 1\right) y_1'^2\right]^{1/2} + y_1'\left[1 + \left(\frac{x_2'}{y_1'}\right)^2\right]^{1/2} + \frac{\frac{2x_2'}{y_1'}(x-x_2') - 2y}{2\sqrt{1 + \left(\frac{x_2'}{y_1'}\right)^2}}\right\}$$

$$- \frac{1}{\sqrt{1 + \left(\frac{x_2'}{y_1'}\right)^2}} \ln\left\{\left[(x-x_2')^2 + y^2 + z^2 + \frac{\frac{2x_2'}{y_1'}(x-x_2') - 2y}{2\sqrt{1 + \left(\frac{x_2'}{y_1'}\right)^2}}\right]\right\} \qquad (39)$$

$$- \frac{1}{\sqrt{1 + \left(\frac{x_1'}{y_1'}\right)^2}} \ln\left\{\left[(x+x_1')^2 + y^2 + z^2 + \left(-\frac{2x_1'}{y_1'}(x + x_1') - 2y\right) y_1\right.\right.$$

$$\left.\left. + \left(\left(\frac{x_1'}{y_1'}\right)^2 + 1\right) y_1'^2\right]^{1/2} + y_1'\left[1 + \left(\frac{x_1'}{y_1'}\right)^2\right] + \frac{\frac{-2x_1'}{y_1'}(x + x_1') - 2y}{2\sqrt{1 + \left(\frac{x_1'}{y_1'}\right)^2}}\right\}$$

$$- \frac{1}{\sqrt{1 + \left(\frac{x_1'}{y_1'}\right)^2}} \ln \left\{ \sqrt{(x + x_1')^2 + y^2 + z^2} + \frac{\frac{-x_1'}{y_1'}(x + x_1') - y}{\sqrt{1 + \left(\frac{x_1'}{y_1'}\right)^2}} \right\}$$

$$I_y = \frac{1}{\sqrt{1 + \left(\frac{y_1'}{x_1'}\right)^2}} \ln \left\{ [(y-y_1')^2 + x^2 + z^2]^{1/2} + \frac{\frac{-y_1'}{x_1'}(y-y_1') - x}{\sqrt{1 + \left(\frac{y_1'}{x_1'}\right)^2}} \right\}$$

$$- \frac{1}{\sqrt{1 + \left(\frac{y_1'}{x_1'}\right)^2}} \ln \left\{ [(y-y_1')^2 + x^2 + z^2 + \left(\frac{2y_1'}{x_1'}(y-y_1') + 2x\right) x_1' \right.$$

$$\left. + \left(\left(\frac{y_1'}{x_1'}\right)^2 + 1\right) x_1'^2]^{1/2} - x_1' \left[1 + \left(\frac{y_1'}{x_1'}\right)^2\right]^{1/2} \right.$$

$$\left. + \frac{\frac{-y_1'}{x_1'}(y-y_1') - x}{\sqrt{1 + \left(\frac{y_1'}{x_1'}\right)^2}} \right\} - \ln \left\{ [x^2 + y^2 + z^2]^{1/2} - x \right\} \qquad (40)$$

$$+ \ln \{[x^2 + y^2 + z^2 + 2xx_1' + x_1'^2]^{1/2} - x_1' - x\}$$

$$+ \frac{1}{\sqrt{1 + \left(\frac{y_1'}{x_2'}\right)^2}} \ln \{[(y-y_1')^2 + x^2 + z^2 + \left(\frac{2y_1'}{x_2'}(y-y_1') - 2x\right) x_2'$$

$$+ \left(1 + \left(\frac{y_1'}{x_2'}\right)^2\right) x_2'^2]^{1/2} + x_2' [1 + \left(\frac{y_1'}{x_2'}\right)^2]^{1/2} + \frac{\frac{y_1'}{x_2'}(y-y_1') - x}{\sqrt{1 + \left(\frac{y_1'}{x_2'}\right)^2}} \}$$

$$- \frac{1}{\sqrt{1 + \left(\frac{y_1'}{x_2'}\right)^2}} \ln \{[(y-y_1')^2 + x^2 + z^2]^{1/2} + \frac{\frac{y_1'}{x_2'}(y-y_1') - x}{\sqrt{1 + \left(\frac{y_1'}{x_2'}\right)^2}} \}$$

$$- \ln \{[x^2 + y^2 + z^2 - 2xx_2' + x_2'^2]^{1/2} + x_2' - x \}$$

$$+ \ln \{[x^2 + y^2 + z^2] - x\} ,$$

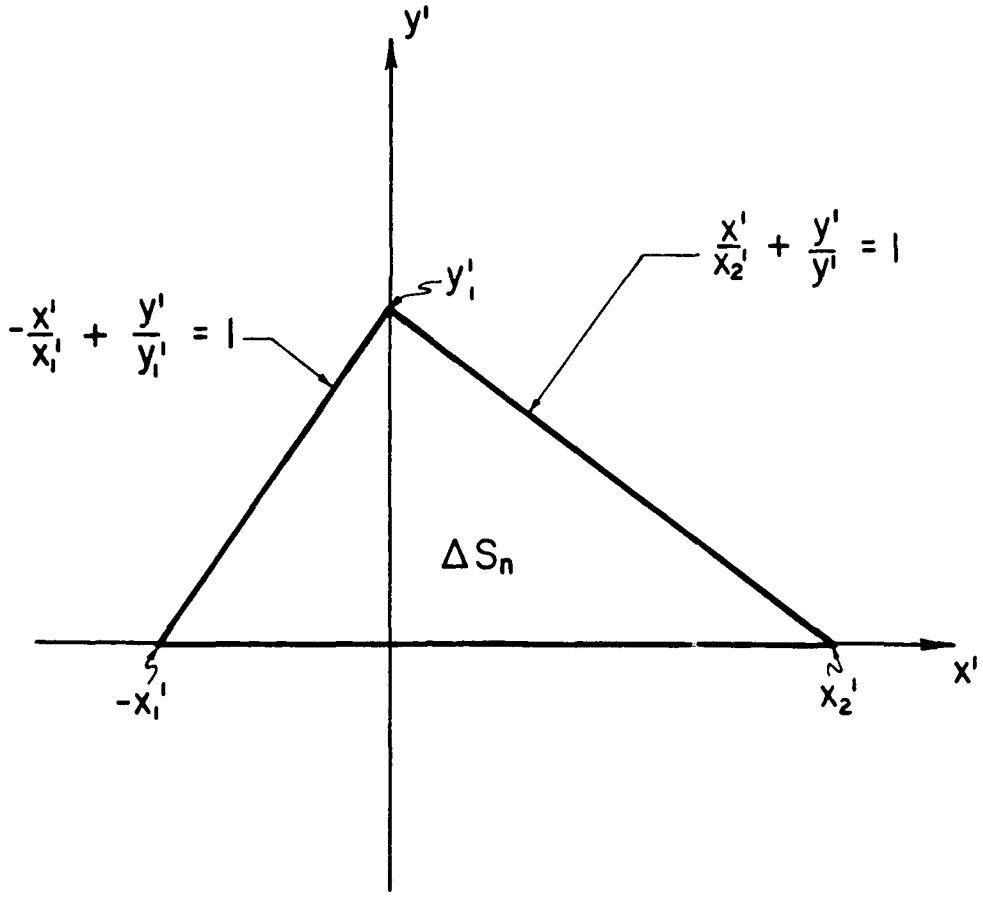

Figure 2. A triangular patch and the coordinates.

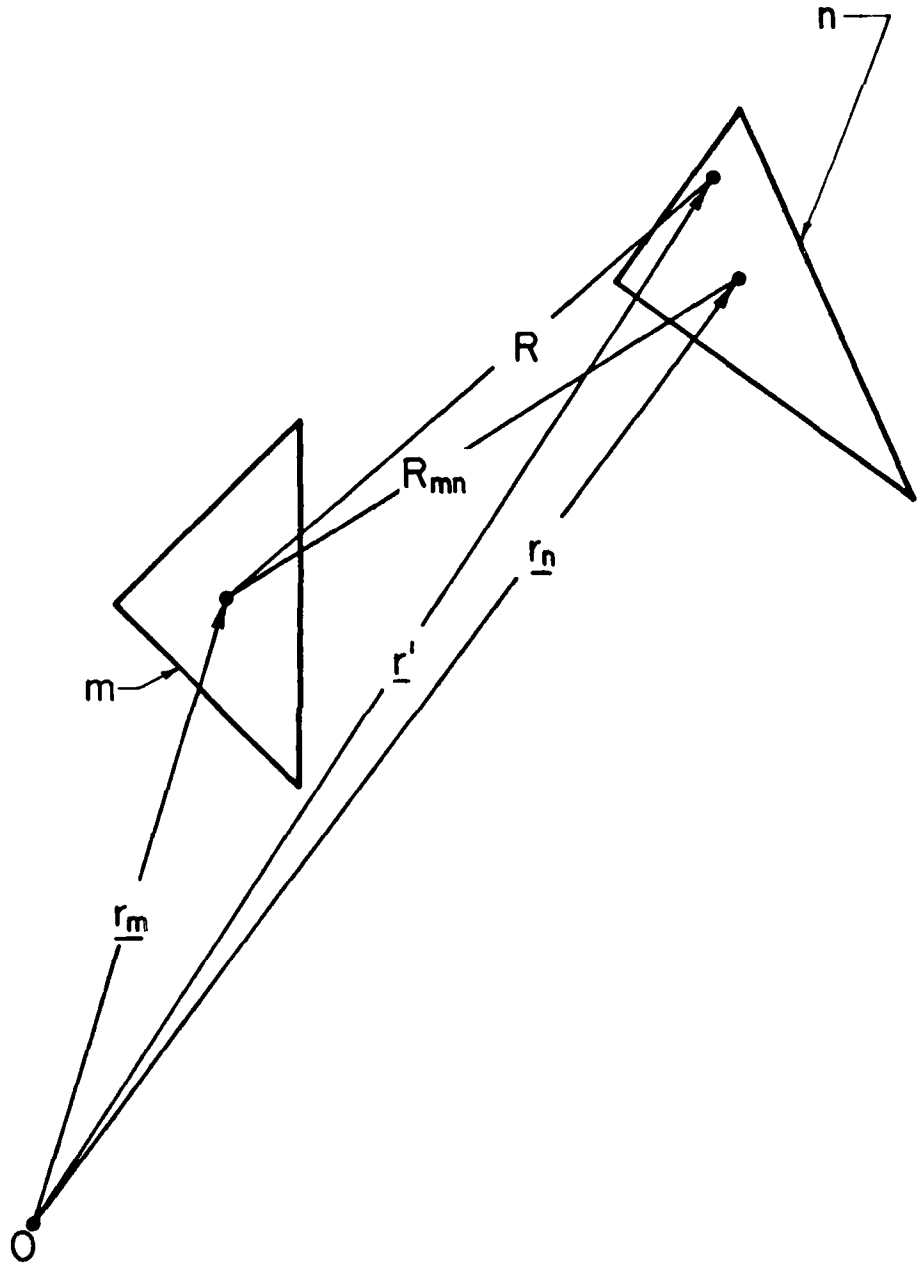

Figure 3. Geometry of the mth and the nth patches.

where x,y,z denote x_m, y_m, z_m, respectively.

Although Equation (38) is an accurate expression for the computation of $\underline{I}_n^n$, it is quite cumbersome. In practice, the simple expression of Equation (33) is quite satisfactory. In fact, all the numerical data included in this report are based on Equation (33). The CPU time required in generating the matrix elements is small, being on the order of 100 seconds for a 192x193 matrix on the CDC CYBER 74 computer at Georgia Tech.

E. Interior Resonance

Interior resonance in electromagnetic scattering has been observed in two types of problems, one due to the simulation by wire-grids [10,11], the other being related to the integral equation used. In both cases, the solution to an integral equation is not unique at the resonance frequency of the interior cavity. Thus, a solution to the interior problem emerges while the exterior problem is being solved.

The latter type of resonance was discussed in detail by Poggio, et al. [12]. A similar phenomenon in acoustics was analyzed by Copley [13] and Schenck [14]. Copley showed that the integral representation of the velocity potential contained the product of $1/(k-k_m)$ and a surface integral, where k is the free space wavenumber and k_m an eigen-value of the interior problem. As $(k-k_m)$ approaches zero, the surface integral must also vanish so that their product will yield a finite value for the velocity potential. Consequently, it becomes increasingly difficult to calculate accurately the ratio of two vanishing quantities as k approaches k_m. Since the accuracy of the computer is limited, numerical inaccuracy will arise at the resonant frequency.

In electromagnetics, a similar mechanism was noted in various integral equation formulations [12,15,16,17]. Harrington [16,17] stated that both electric-field and magnetic-field integral equations failed at frequencies corresponding to the resonant frequencies of the interior problem. The present algorithms employ the magnetic field integral equation and are therefore expected to exhibit difficulties at the interior resonance frequencies. In fact, a careful search near the

first eigen frequency of a sphere of radius "a" located at ka=2.744 revealed an erratic behavior in the calculated backscatter cross-section around the value of ka=2.89, as shown in Figure 4.

The distinctive feature of the internal resonance in Figure 4 is the rapidity and sharpness of the variation of the radar cross-section versus frequency. Because of the slight frequency shift and the narrowness of the resonance bandwidth, this resonance escaped an earlier inquiry into this phenomenon. Although the resonance has shifted, the radar cross-section curve off resonance does not show any significant shift one way or the other. Therefore, this shift of resonance can not be explained as being due to the effective size of the sphere simulation. It is probably due to the surface-patch algorithm, which may be less sensitive to resonance phenomena than other algorithms.

It is now clear that internal resonance presents a numerical problem in the present algorithm over a narrow bandwidth near the resonance frequency. Correction of this deficiency can be carried out by following either of the two approaches outlined by Mautz and Harrington [16,17]. These methods involve the use of a modified integral equation, the combined field or the combined source, for which the solution is unique.

F. The Basis and Weighting Functions

The basis function used in the present approach was defined in Equations (3) through (7). It is natural to ask whether other basis functions can be used to any advantage. For example, it is sometimes possible to orient all the basis vectors perpendicular to a fixed coordinate axis instead of the incident wave polarization. This was tried for the case of spheres with a surprising result. The output data are nearly identical whether the basis vectors are oriented according to the incidence polarization or a fixed coordinate. No other geometry was tested because of the difficulty in defining a basis vector perpendicular to both the surface normal vector and the fixed coordinate. We have not been able to obtain a satisfactory explanation for this discovery during our brief examination of this problem.

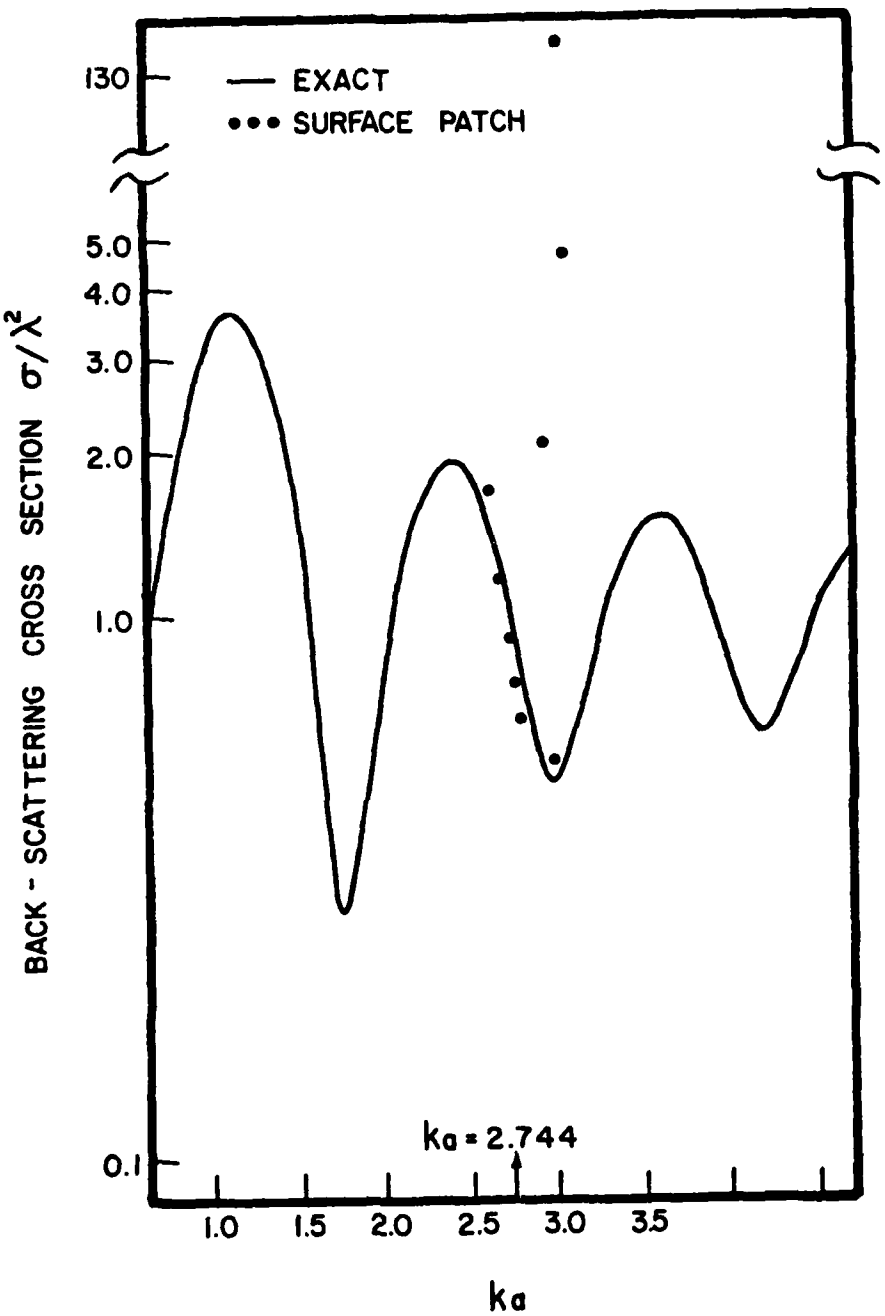

Figure 4. Erratic numerical data near the interior resonance frequency of a conducting sphere of radius a.

Basis functions other than the subsectional pulse function have been considered in the present study. These alternate basis functions included the triangular and sinusoidal pyramid functions. The possibility of extending these subsectional bases over more than one patch was also considered. Since the current is continuous for a conducting body having a closed surface, the triangular and sinusoidal pyramid bases must be extended to cover more than one patch in order to achieve continuity for the current.

Figure 5 shows a triangular pyramid basis function peaked at the center of the bisectors of the center patch. Assuming that all the patches are organized to share one side with each of the three adjacent triangles, we can establish a basis function which is centered in each patch and declines to zero at the centers of the adjacent patches. Note that the shaded and unshaded triangular pyramids in Figure 5 only represent the magnitude of the current, not its polarization.

One problem with the shaded basis function from the shaded to the unshaded pyramid in Figure 5 is that the current is zero on the vertices of the triangular patch. It is therefore desirable to modify the basis function by extending it from 2, 3, 4, to 2', 3', and 4', respectively. The decay of the basis function from 1 to 2, 3, and 4, (or 2', 3', and 4') can be changed from linear to sinusoidal if it offers any computational advantages.

The weighting function used in the present approach is the Dirac-delta function according to Equation (9). If a flat pulse function is used, the matrix element is then given by

$$Z_{mn}^{ij} = \Delta S_m \delta_m^n \cdot \delta_j^i - \frac{1}{2\pi} \underline{U}_m^j \cdot \hat{n}_m \times \{ \underline{U}_n^i \times \int_{\Delta S_m} [\int_{\Delta S_n} \nabla' \Phi(\underline{r},\underline{r}') ds'] ds \} \tag{41}$$

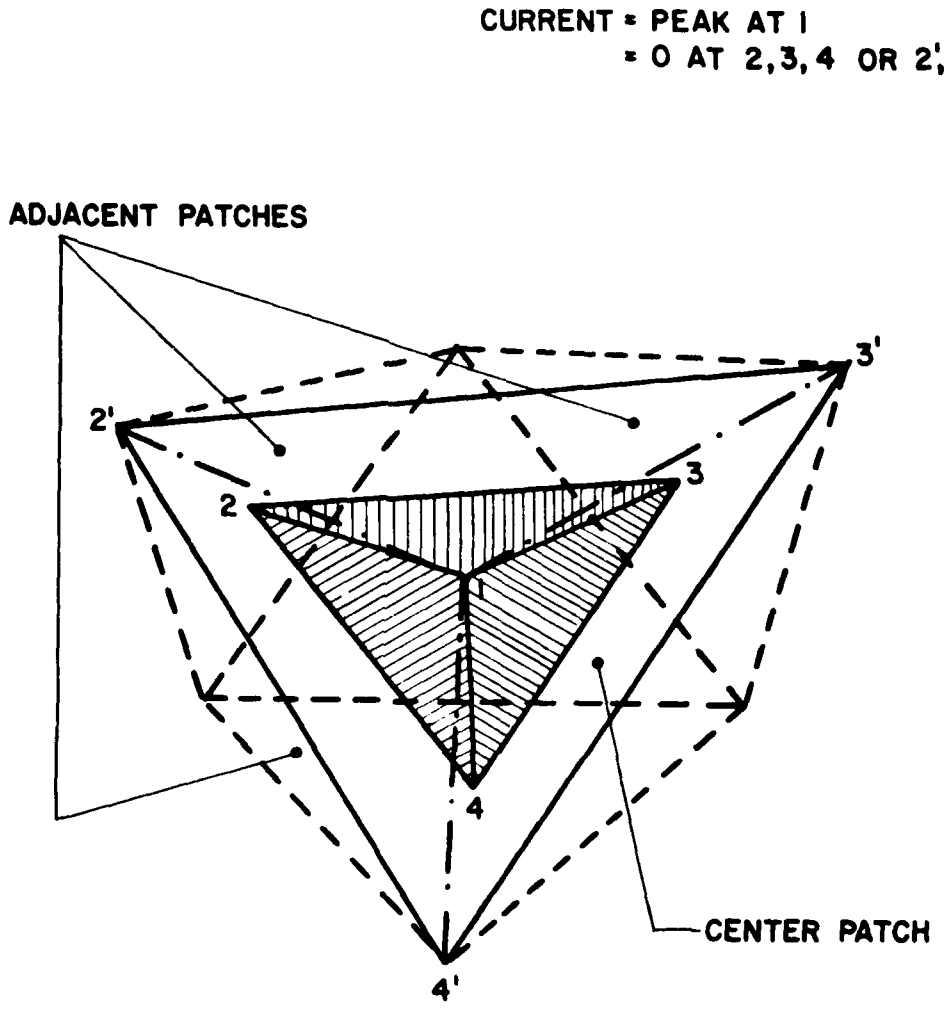

Figure 5. Two triangular pyramid basis functions centered at point 1 of the center patch.

Equation (41) now involves a double integration. The integration with respect to s' can be approximately expressed in closed form according to Equations (38) - (40). The next step, integration with respect to s, appears difficult and must be computed numerically.

The Dirac-delta function can be used as a weighting function for the triangular pyramid basis function. In fact, six out of the seven major wire analysis programs use Dirac-delta functions as the weighting function and this method is referred to as collocation [18]. In this manner, the complexity of the triangular pyramid basis function can be drastically reduced.

SECTION III
NUMERICAL TESTING

Based on the study described in the preceeding section, two computer programs, SCT51 and SCT52, were developed for numerical testing. These two computer programs have been described in a separate document [19] and thus their descriptions will not be repeated herein. The program SCT51 applies to arbitrarily-shaped scatterers without matrix integration and the program SCT52 applies to symmetrical scatterers with the incident wave propagating along the plane of symmetry.

Numerical computations have been performed previously for conducting spheres of various sizes [4]. Thus, it is of interest to consider other geometries and the scatterers studied in this report include prolate spheroids and finite length circular cylinders and rectangular cylinders. The results of the computations were then compared with existing data in the literature. While excellent agreement between the data and the computations has been observed, there was an apparent discrepancy with respect to polarization in some of the cases which were considered. Namely, our TE (Transverse Electric) calculation may agree with known data of TM (Transverse Magnetic) case, and our TM case may agree with the known TE data in the literature. In fact, our results agree with some sources and disagree with some other sources as far as the incidence polarization is concerned. We have examined the set-up of the incidence wave in our computer program and have not found any error. At this point, we tentatively assume that the discrepancy is due to confusion in data presentation with respect to denoting the polarization. A further examination of the literature may resolve this apparent notation problem.

The incidence polarization problem emerged only when it affected the results. In many instances, the geometries are symmetrical and the scattering characteristics are identical in the two principal planes. There is also a possibility of error in the definitions of the axes to which the TE and TM modes are referred. The axis was defined in all the

data presented in the literature but this definition could be a potential source of error.

In order to resolve the polarization problem, a series of measurements is planned in early 1980 when the compact range at Georgia Tech will be available for scattering measurements.

With the foregoing discussion in mind, we proceed to present the numerical results, which when we ignore the discrepancies in polarization in some cases, are in good agreement with existing data in the literature.

The computation for prolate spheroids employed a 54-point, 96-patch spheroidal structure described in Reference 4, which is easily elongated in one dimension to generate the desired prolate spheroid. Figures 6 through 8 show the comparison of the back-scattering cross-section resulting from the present calculation and the data from Moffatt, et al. [20,21]. The minor axis a of the patched prolate spheroid is determined by its "effective" value, which is calculated by dividing the circumference by 2π.

The backscatter from a finite length circular cylinder was calculated using the program SCT52 and the results are compared with data in the literature [22] for E-plane and H-plane incidence. Again the question of effective diameter of the cylinder arises. Figure 9 shows how the finite circular cylinder was simulated with triangular patches. Figure 10 shows how the patched cylinder is related to the circular cylinder. Obviously, a cross-section inscribed on circle is a less reasonable choice than the cross-section area corrected to a circle. Indeed, better results were obtained by the method of cross-section area corrected to a circle as shown in Fgures 11 and 12.

Figures 13 and 14 show the comparison of the computed results for a finite rectangular cylinder with the calculation by Tsai, et al [23,24], who referred to the rectangular cylinders as boxes. SCT52, which takes advantage of the symmetry of the problem, was employed in this calculation. Tsai's calculation also utilized the symmetry of the scatterer. Note that a 60 x 60 matrix was used in the present calculation while a 100 x 100 matrix was used by Tsai.

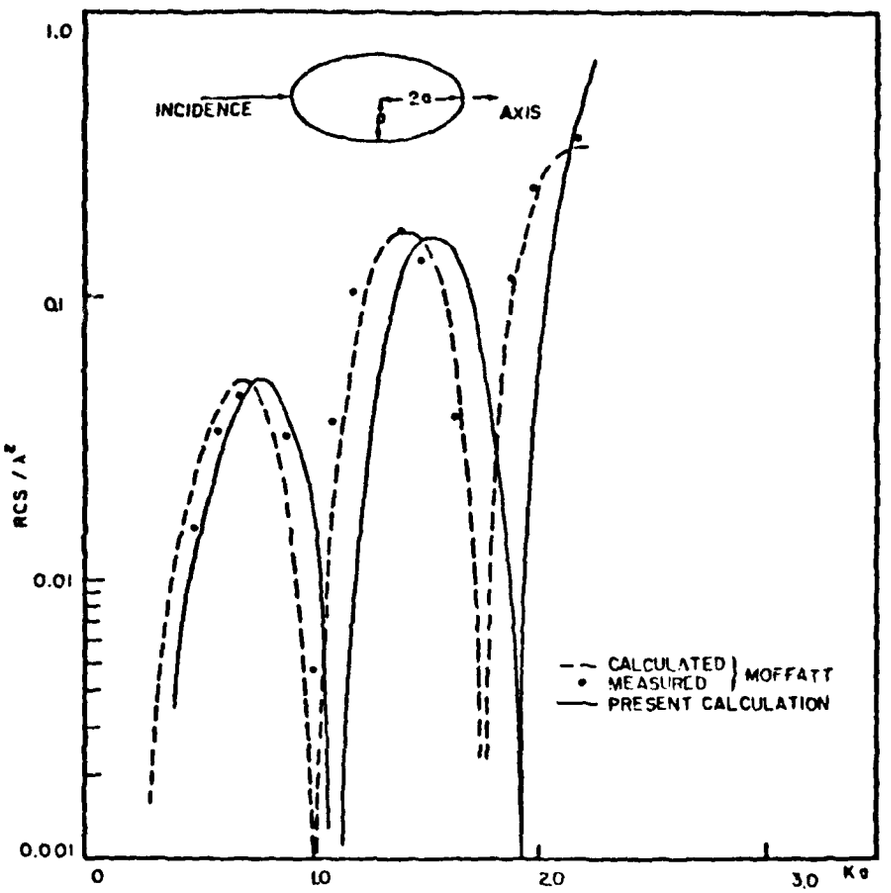

Figure 6. Backscattering cross section of a conducting prolate spheroid with incidence parallel to the major axis.

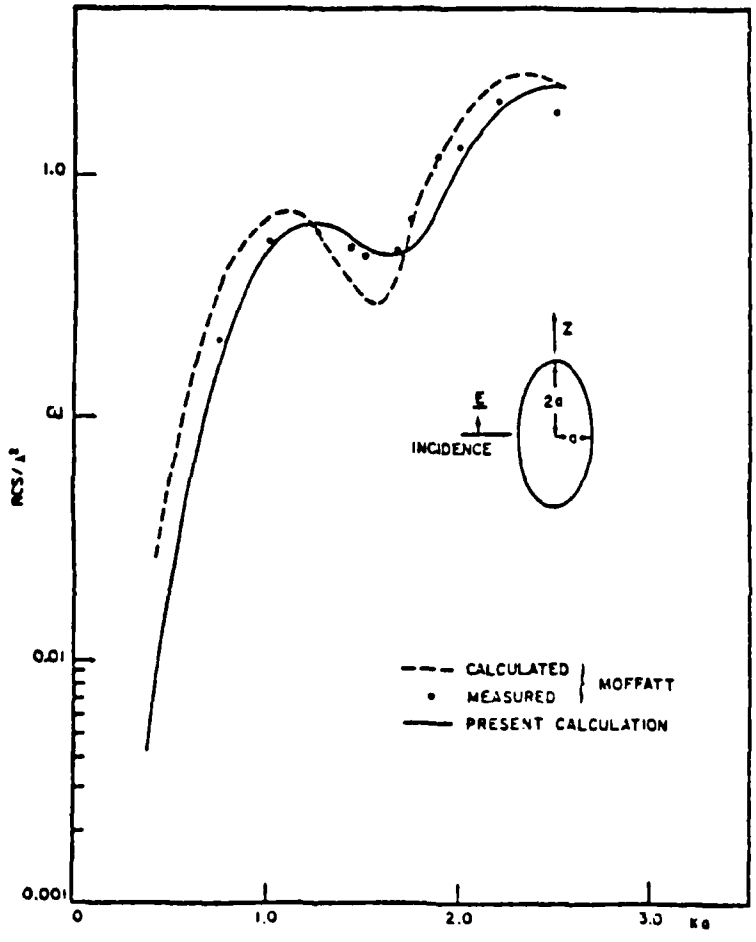

Figure 7. Backscattering cross section of a conducting prolate spheroid with incidence perpendicular to the major axis -- TE polarization.

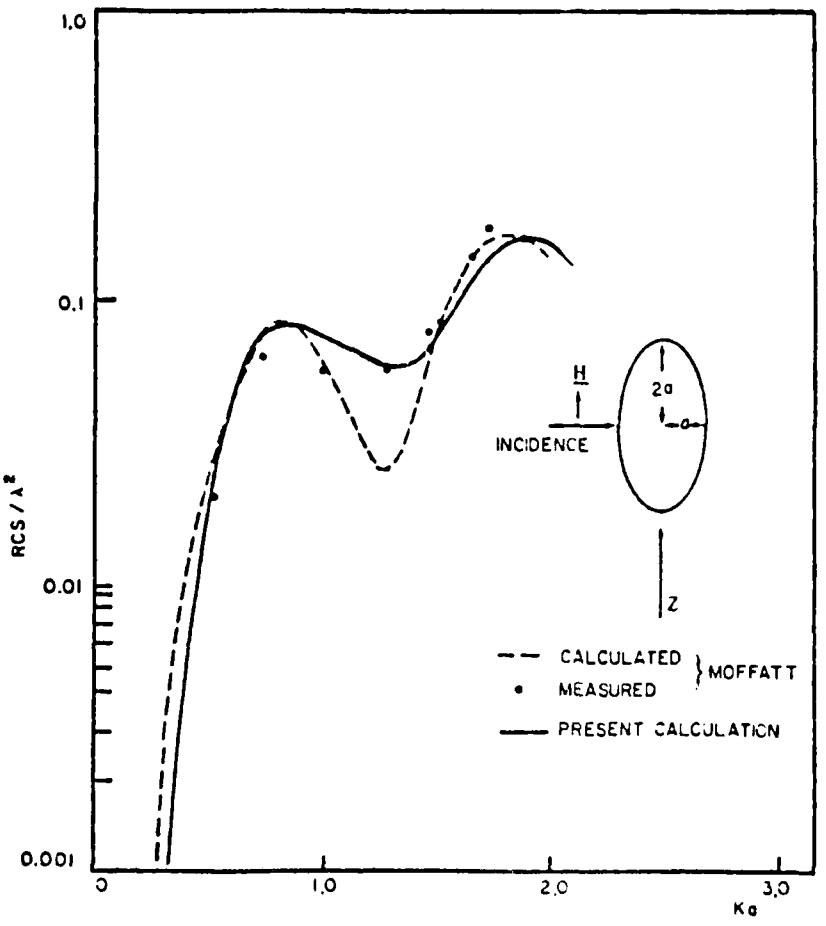

Figure 8. Backscattering cross section of a conducting prolate spheroid with incidence perpendicular to the major axis -- TM polarization.

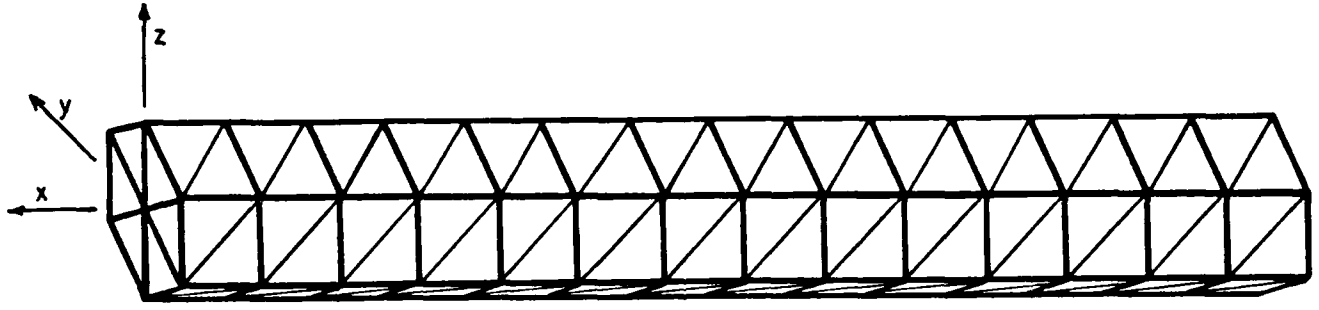

Figure 9. A circular finite cylinder simulated with triangular patches for computation using SLT52.

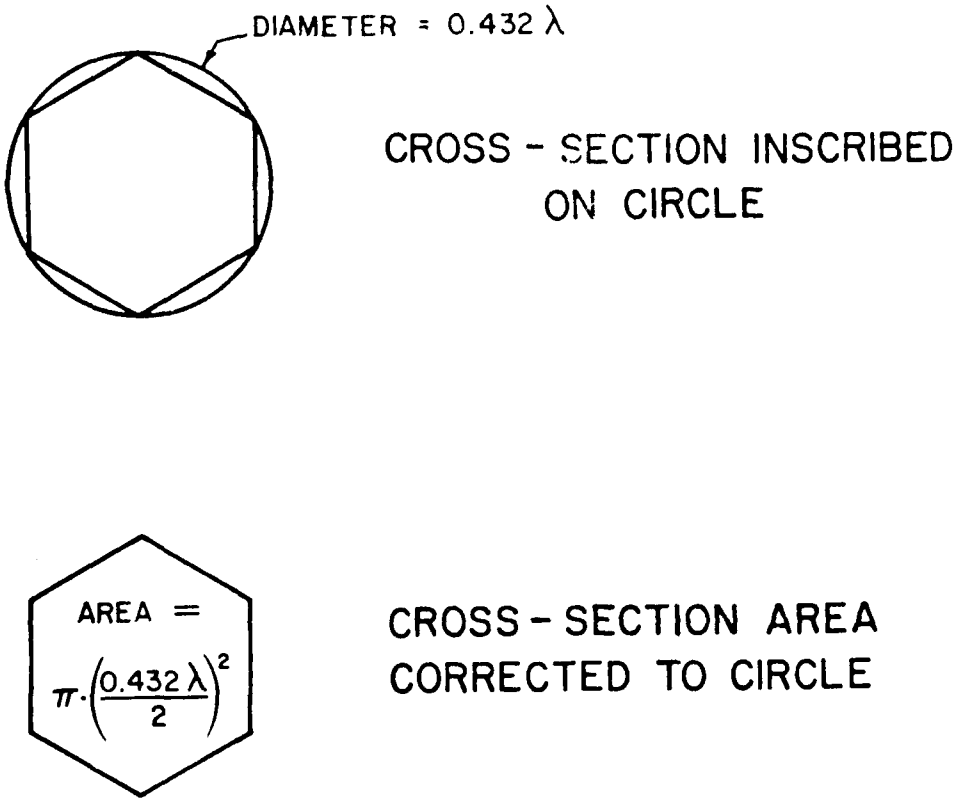

Figure 19. Cross sectional views showing two methods in handling the effective diameter of the circular cylinder.

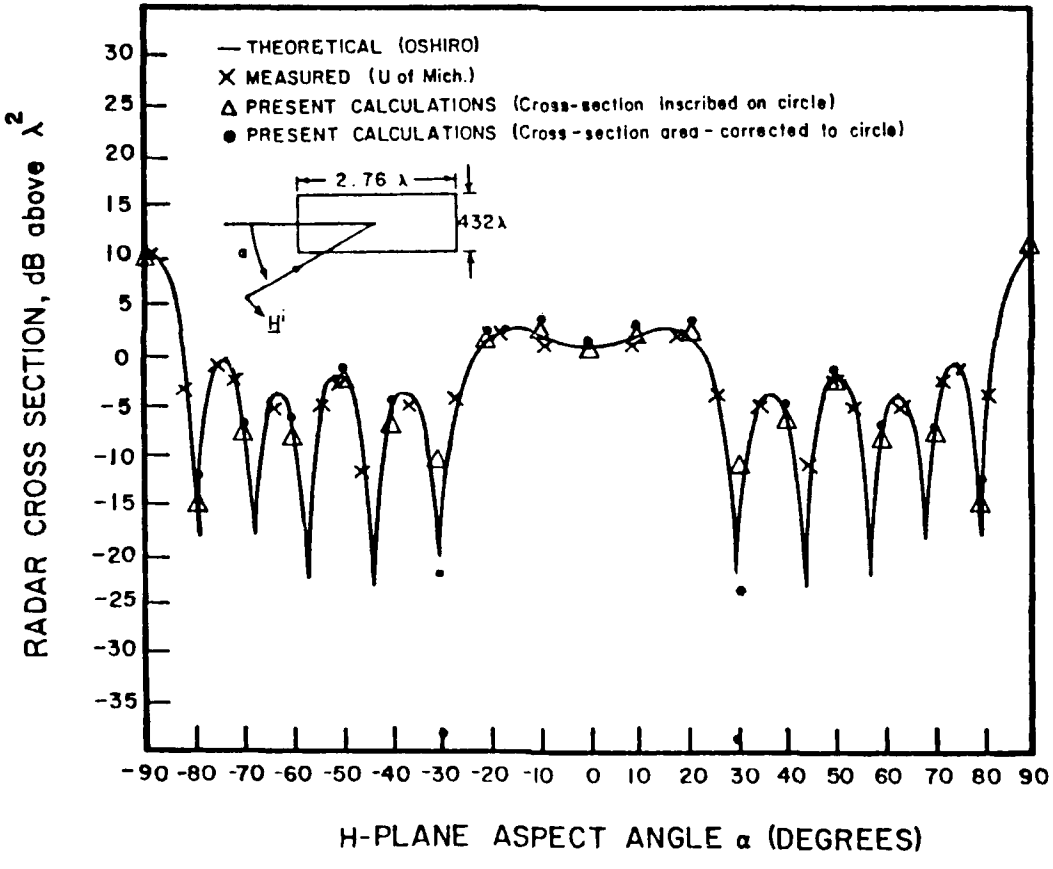

Figure 11. Backscattering cross section of a finite circular cylinder in the H-plane.

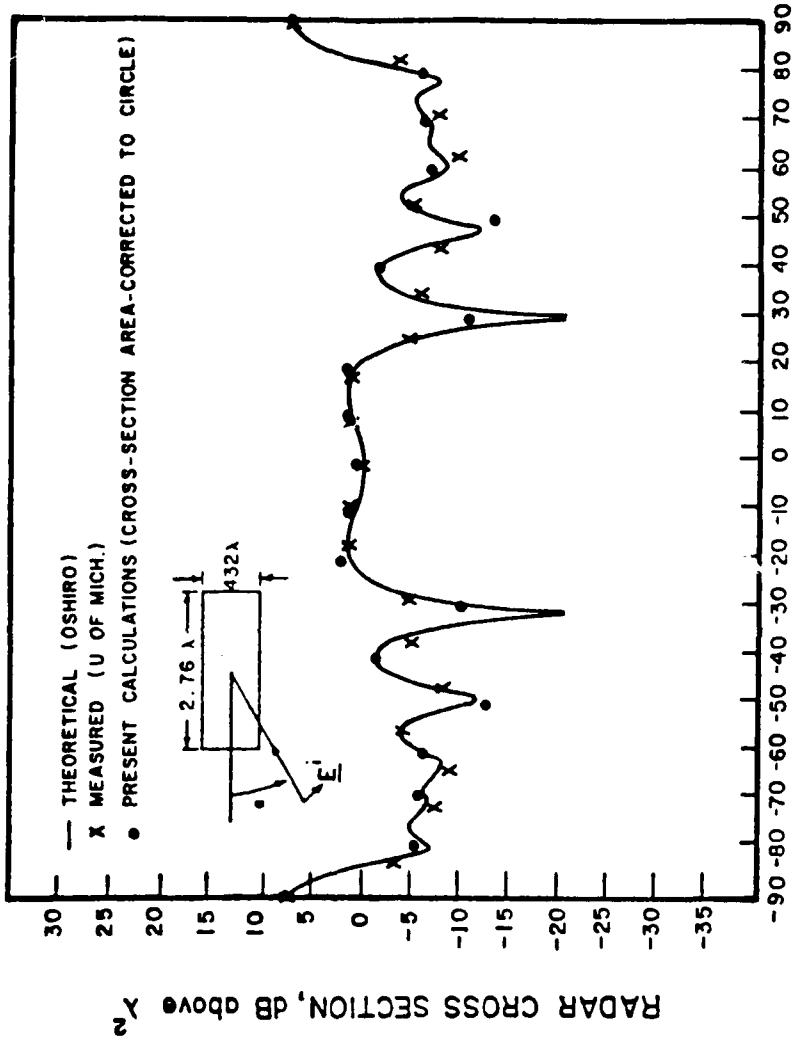

Figure 12. Backscattering cross section of a finite circular cylinder in the E-plane.

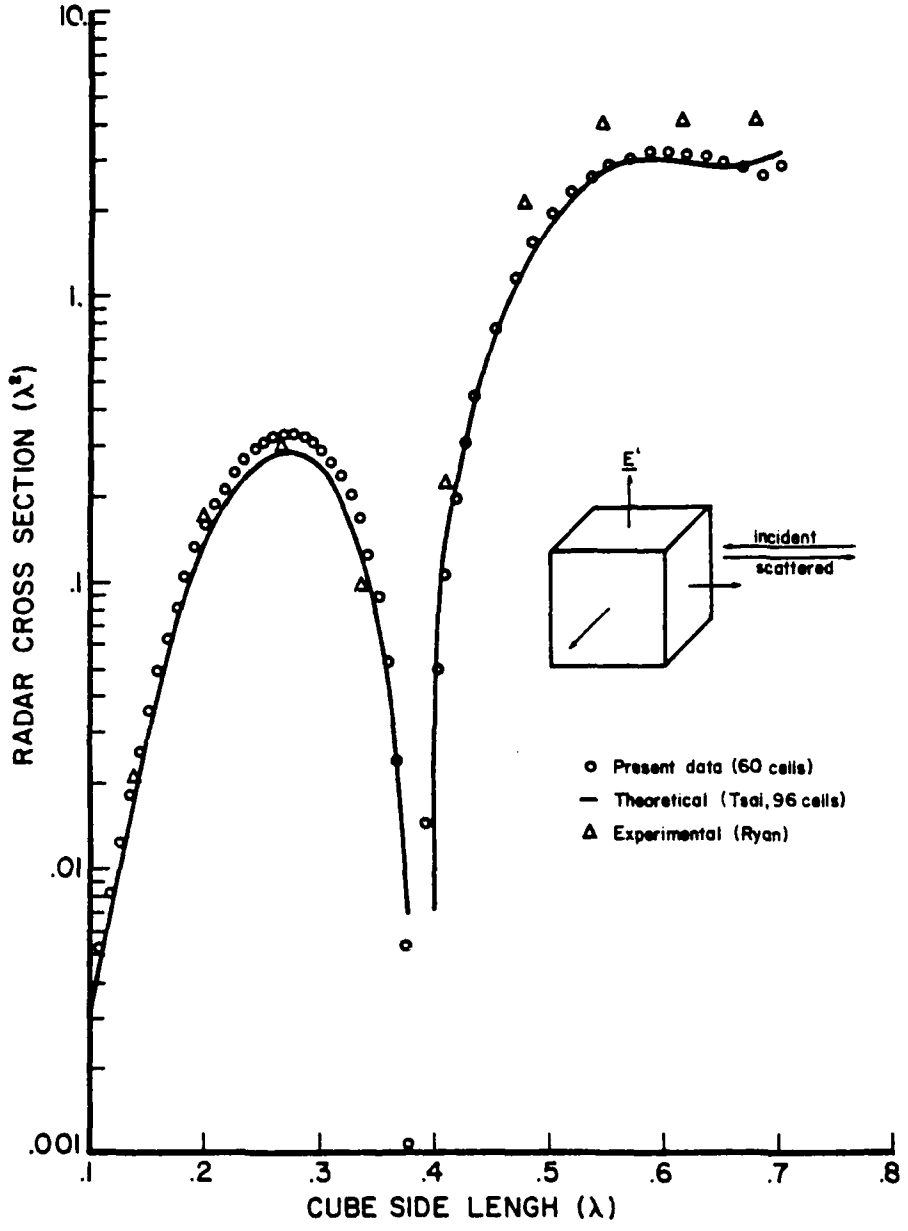

Figure 13. Comparison of the computed radar cross section of a conducting box with other known data.

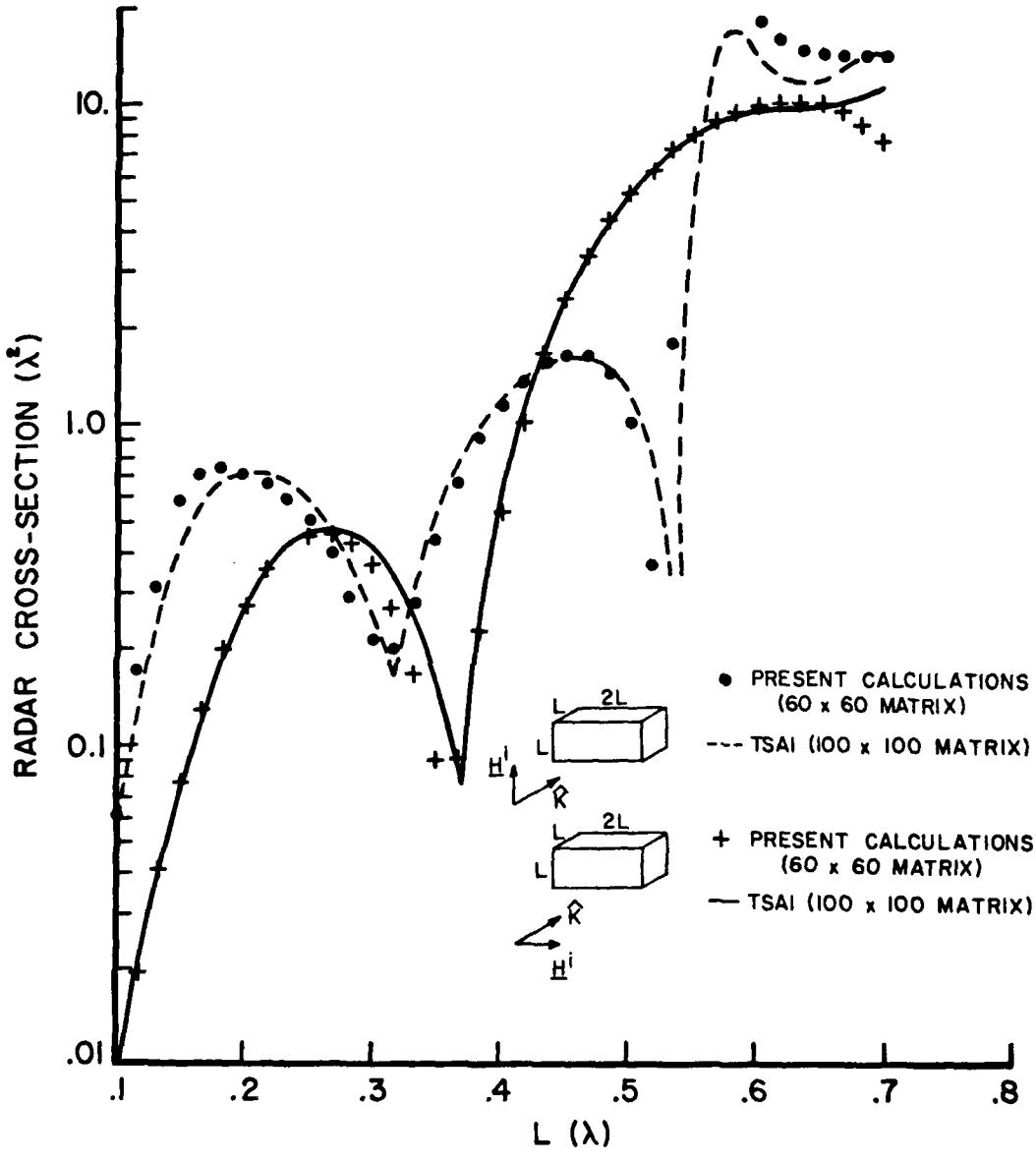

Figure 14. Comparison of the computed radar cross section of a conducting rectangular cylinder with other known data.

Several salient features were observed in the numerical testing of the Georgia Tech computer program. The computer program is capable of generating accurate scattering data as long as the patch sizes are such that the centers of the adjacent triangular patches are spaced a quarter wavelength or less. Geometries involving sharp angles such as the boxes and finite circular cylinders can be handled without degradation in accuracy. The computational speed and central memory requirement are dependent on the number of patches used in the simulation. For a 96-patch spheroid, which nearly occupies the full central memory of the CDC Cyber 74 computer at Georgia Tech, one run using SCT51 at a single frequency and one incidence angle takes about 150 CPU seconds. When SCT52 is used for a symmetrical geometry, both the central memory and CPU time is reduced by three-fourths.

It is also of interest to compare the numerical advantages of the surface-patch modeling and the wire-grid modeling approaches. Although a number of wire-grid algorithms have been developed [18], there appears to be no calculations with wire algorithms for the geometries presented in this report. A wire-grid model for a sphere, originally calculated by J.H. Richmond, was reported in Reference 12. This wire-grid model employed an earlier algorithm by Richmond, yielding only fair results. A more critical comparison was performed at Georgia Tech [4] with Richmond's latest refined wire algorithm [6]. It was shown in this comparison that the present surface-patch approach was able to produce data of better accuracy while using fewer linear equations and less execution time. The wire approach employed 194 equations, and required a 27-second compilation time and a 237-second execution time. The surface-patch approach employed 192 equations, and required a 8-second compilation time and a 150-second execution time. However, Richmond's reaction integral equation approach has one major advantage. Its matrix is symmetrical and as a result its central memory requirement is only about 60 percent of that for the surface-patch algorithm. This advantage of the reaction integral equation algorithm is apparently not shared by other wire algorithms and was not mentioned in the detailed comparison study of various wire-grid approaches [18].

SCT52, the surface-patch algorithm for symmetrical scatterers, reduces the execution time and central memory requirements by 75 percent. When there is two-plane symmetry, this reduction is 94 percent. Thus, for the sphere, in which two-plane symmetry exists, the exectuion time is 9 seconds and the central memory size will be one sixteenth of that required by SCT51 or one-eighth of that required by Richmond's wire algorithm.

No comparison has been made between wire algorithms and the surface-patch algorithms for geometries other than the sphere. The accuracy and convergence of the surface-patch algorithm discussed herein surpass those of the wire algorithms so that a detailed comparison with wire algorithms is not of high priority in the research program. The effort in generating correct data for various geometries using the wire approach is estimated at one to two person-months. There will also be the question of what size of diameter to choose for the wires and how these wires should be organized in the simulation. The fact that the scattering characteristics depend on the wire radius to be chosen has already seriously hindered the wire-grid approach for surface modeling. Now that the surface-patch approach has demonstrated its accuracy for several important types of scatterers, including some with sharp edges, the advantages of the surface-patch approach over the wire-gird approaches are evident.

SECTION IV

DEVELOPMENT OF A COMPUTER PROGRAM FOR THIN-SHELL PROBLEMS

It is well known that the magnetic field integral equation encounters numerical instability problems when used for thin-shell scatterers [25]. This difficulty can be overcome by using the reaction integral equation [26] and electric field integral equation [27] or others [25,28,29]. However, computations in the literature invariably are limited to the simple case of a rectangular conducting plate and a dihedral corner reflector. There is no indication that any of these methods can be readily applied to other geometries.

In the process of developing a computer program for the scattering of arbitrarily-shaped thin shell structures, two approaches were taken in this study. A reaction integral equation approach was initially investigated but was not completed because of large CPU time requirements in the numerical computation of matrix elements. An electric field integral equation approach was then adopted and a computer program coded and debugged. Both of these approaches are discussed in the following paragraphs.

A. Reaction Integral Equation Approach

The reaction integral equation has been applied to the cases of a rectangular plate and a dihedral corner reflector [26]. The possibility of using this approach for arbitrarily-shaped scatterers is examined herein. The major difficulty in this approach lies in the difficulties in the integration to obtain the matrix elements given by

$$Z_{mn}^{ij} = -\int_{\Delta S_m}\int_{\Delta S_n} \underline{J}_m^i \cdot \underline{E}_n^j \, ds'ds \tag{42}$$

where $\underline{J}_m^i$ = basis function of i^{th} polarization in the m^{th} patch,

$\underline{E}_n^j$ = electric field due to the basis function of i^{th} polarization in the n^{th} patch,

$\Delta S_m, \Delta S_n$ = surfaces of the m^{th} and n^{th} triangular patches.

Strictly speaking, Equation (42) involves triple integrations as $\underline{E}_n^j$ must also be evaluated by an integration process. Presently, there appears to be no closed-form expression for the field due to a triangular current patch. Even in the case of a finite line source, the sinusoidally excited dipole is probably the only one with a simple closed-form expression for the near-zone field [6]. In order to compute $\underline{E}_n^j$ in Equation (42), two integration methods were tried. The first method employs modern numerical integration techniques, and the second method is based on the approximation of the surface current with several line current elements.

In the numerical integration technique, the definite integral is expanded into a finite series which can be computed numerically [30]. Specifically, the integration of a function over a triangular area can be carried out with a 64-point formula [30]. 64 points in the triangle are pre-selected according to a simple arithmatic formula and the values of the integrand at these points are then computed. The value of the integral is then obtained by summing up the product of these 64 sampled integrands and a predetermined weighting function of simple arithmatic form.

The accuracy of the numerical integration depends on how rapidly and how frequently the value of the integrand varies in the area of integration. The 64-point algorithm was checked with several known functions and the accuracy of this algorithm was quite impressive. For example, Table I shows the comparison between the exact values and the results of numerical integration for the integral

$$\int_0^1 \int_0^{1-x} \sin\omega x \, dy \, dx. \tag{43}$$

As can be seen, even when $\omega=10$, the 64-point algorithm is highly accurate.

Although this integration algorithm is highly accurate, it is inefficient. The total subroutine contains only 17 lines of short and simple arithmetic expressions, as well as an 8x8 "DO" loop. It takes about 0.08 CPU second to run one case in Table I. Consequently,

TABLE I

ACCURACY OF THE 64-POINT NUMERICAL INTEGRATION ALGORITHM

$$\text{Integral tested} = \int_0^1 \int_0^{1-x} \sin \omega x \, dy \, dx.$$

ω	Exact	Numerical integration
0	0	0
1	0.1585290152	0.1585290
10	0.1054402111	0.1054402
100	0.0100506366	0.05372281
1000	0.0009991731	-0.008012371

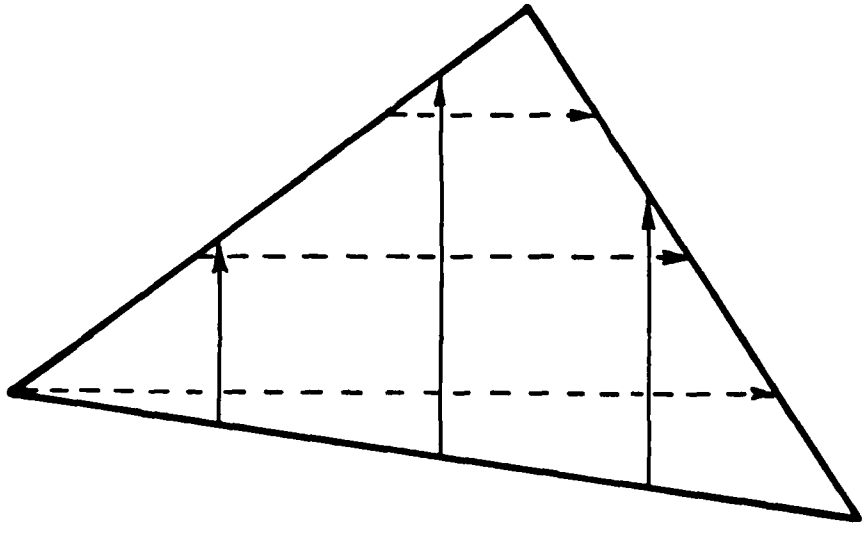

Figure 15. An arbitrary triangular current patch being approximated with orthogonal current filaments.

considerable restraint must be exercised in applying this technique to the evaluation of matrix elements in Equation (42). Since we were unable to obtain a closed form expression for $\underline{E}_n^j$ in Equation (42) analytically, we chose to approximate the patch current with current filaments as shown in Figure 15. Obviously, the higher the number of filaments included in the process, the more accurate will be the approximation.

The expressions for the electric field radiated from a line current having a sinusoidal distribution were well documented by Schelkunoff and Friis [31]. Because of the symmetry of a straight line current, the radiated field is constant around the axis of the line current. The radiated field therefore consists of two components, one parallel to the current and one perpendicular to the current. There is no Φ component if a cylindrical coordinate is assigned with the current along the z-axis. A check of the formulas for E_ρ and E_z showed that E_ρ was an exact expression. However, the expression for E_z was not exact as implied. In Equations (12) through (40) of Reference 31, the term

$$\frac{1}{j\omega\varepsilon} \frac{\partial I}{\partial z'} \frac{\partial \Psi}{\partial z'} dz' \tag{44}$$

was omitted in the derivation. The exact expression should read

$$dE_z = \frac{1}{j\omega\varepsilon} \left(\frac{\partial^2 \psi}{\partial z'^2} + \frac{\partial I}{\partial z'} \frac{\partial \psi}{\partial z'} + \beta^2 \psi \right) I(z')dz' \tag{45}$$

It was noted that Equation (45) without the term of Equation (44) is Pocklington's integral equation [32]. On the other hand, Equation (45) was employed by Kyle [33], Richmond [34], Harrington [35], and Thiele [36] in their thin-wire computations. In the present study, Pocklington's integral was chosen so that all the formulations for a line current source were based on Reference 31.

Figure 16 shows a comparison between the present calculation and the calculated data in Reference 26 for the mutual impedance between two rectangular dipoles. The present calculation employed three filament approximations for triangular surface patches. Each rectangular patch

S_z/λ	S_y/λ	Wang Richmond Gilbreath	Present Calculation
0	0.25	39.07 - j22.49	38.92 + j70.31
0	0.50	- 8.659 - j26.75	- 8.589 - j26.56
0.25	0.25	29.54 - j 9.070	29.42 - j36.79
0.50	0.50	- 9.568 - j 6.65	- 9.484 - j 6.574

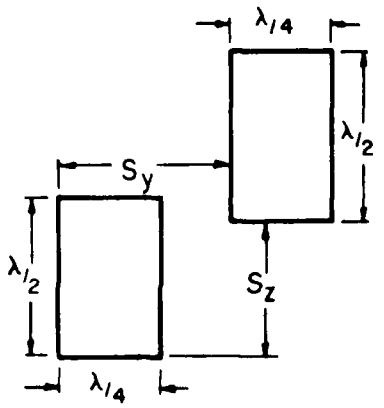

Figure 16. Comparison of computed mutual impedances between two rectangular dipoles.

was divided diagonally into two triangular patches. The agreement with data of Wang, Richmond, and Gilbreath [26] was good as long as the dipoles are spaced one quarter wavelength away. For closely spaced dipoles, more current filaments are needed in the approximation.

This combined analytical-numerical method made it possible to reduce drastically the computational time required for the matrix element to about 1/20 of the time needed for the previous numerical integration. However, the requirement for computational time was still prohibitively high. There appears to be no readily available technique to reduce the CPU time to an acceptable level. The course of research was then turned to the electric field integral equation approach.

B. Electric Field Integral Equation Approach

The electric field integral equation usually takes the following form [12]

$$\hat{n} \times \underline{E}^{inc}(\underline{r}) = \frac{1}{4\pi j\omega\varepsilon} \hat{n} \times \int_s \{-\omega^2 \varepsilon\mu \underline{J}_s(\underline{r}')\phi(\underline{r},\underline{r}') + [\nabla'_s \cdot \underline{J}_s(\underline{r}')]\nabla'\phi(\underline{r},\underline{r}')\}\, ds' \qquad (46)$$

where most of notations have been defined in Equation (1) and

$\underline{E}^{inc}(\underline{r})$ = incident electric field,

$\nabla'_s = \hat{t}_1 \frac{\partial}{\partial t_1} + \hat{t}_2 \frac{\partial}{\partial t_2}$,

$\hat{t}_1$, $\hat{t}_2$ are two orthonormal unit vectors on the surface S.

We denote the right-hand side of Equation (46) with an operator form $X(\underline{J}_s(\underline{r}'))$ and rewrite Equation (46) as

$$X(\underline{J}_s(\underline{r}')) = \hat{n} \times \underline{E}^{inc}(\underline{r}) \qquad (47)$$

We then expand the surface current $\underline{J}_s(\underline{r}')$ according to Equations (3) through (7) and employ the method of moments [35] by performing the scalar product according to Equations (9) and (10). The resulting system of linear equations is

$$\sum_{j=1}^{2} \sum_{n=1}^{N} I_n^j A_{mn}^{ij} = \hat{n}_m \times \underline{E}^{inc}(\underline{r}_m) \cdot \underline{U}_m^i \tag{48}$$

$$i=1,2; \quad m=1,\ldots N,$$

where for $m \neq n$

$$A_{mn}^{ij} = A_{1mn}^{ij} + A_{2mn}^{ij} \tag{49}$$

$$A_{1mn}^{ij} = \frac{1}{4\pi j\omega\varepsilon} \underline{U}_m^i \cdot \hat{n}_m \times \Delta S_n \phi(\underline{r}_m, \underline{r}_n) \{-\omega^2 \varepsilon\mu \underline{U}_n^j + [-jk - \frac{1}{r_{mn}}] \frac{1}{\underline{r}_{nnj} \cdot \underline{U}_n^j} \hat{r}_{mn}\} \tag{50}$$

$$A_{2mn}^{ij} = \frac{1}{4\pi j\omega\varepsilon} \underline{U}_m^i \cdot \hat{n}_m \times \Delta S_n \phi(\underline{r}_m, \underline{r}_n)(jk + \frac{1}{r_{mn}}) \frac{\hat{r}_{mn}}{\underline{r}_{nnj} \cdot \underline{U}_n^j} \tag{51}$$

for $m=n$

$$A_{mn}^{ij}\Big|_{m=n} = \frac{1}{2}\sqrt{\frac{\mu}{\varepsilon}} (1-e^{-jkr_n}) \sum_{j=1}^{2} (1-\delta_j^i)(2i-3) \tag{52}$$

$$r_n = \sqrt{\frac{\Delta S_n}{\pi}}$$

In the foregoing derivation, the surface gradient operator ∇'_s is approximated by

$$\nabla'_s \underline{J}_n(\underline{r}') = \frac{\partial I_n^1}{\partial t_n^1} + \frac{\partial I_n^2}{\partial t_n^2} \approx \frac{I_n - I_{n1}^1}{\underline{r}_{nn1} \cdot \underline{U}_n^1} + \frac{I_n^2 - I_{n2}^2}{\underline{r}_{nn2} \cdot \underline{U}_n^2} \quad , \tag{53}$$

where n1 and n2 are the indices for two patches adjacent to n and are chosen for the evaluation of the gradient of I_n^1 and I_n^2. Note that the accuracy of Equation (53) depends on the local curvature of the surface S. For a flat plane, Equation (13) is most accurate because the polarizations of the first basis vectors $\underline{U}_n^1$ and $\underline{U}_{n1}^1$ are identical; so are the polarizations for the second basis vectors $\underline{U}_n^2$ and $\underline{U}_{n1}^2$. These relations also hold for patch n2. $\underline{r}_{nm1}$ and $\underline{r}_{nm2}$ in Equation (53) are the vectorial distances between the centers of patch n and patches n1 and n2, respectively, as shown in Figure 17.

When one side of the n^{th} triangular patch is an edge, the basis vectors on this patch are organized to orient $\underline{U}_n^1$ to be perpendicular to the edge. $\underline{I}_n^1$, being perpendicular to the edge, is therefore zero in magnitude. $\underline{r}_{nn1}$ is reduced to the case in which the area of patch n1 is zero. In other words, $\underline{r}_{nn1}$ runs from the bisecting piont on the edge side to the center of the triangle.

A generalized computer program based on the foregoing analysis has been coded. There are many similarities between the new thin-shell program and SCT51 program using the magnetic field integral equation. Numerical testing of the thin-shell computer program will be conducted and the results will be included in the final report.

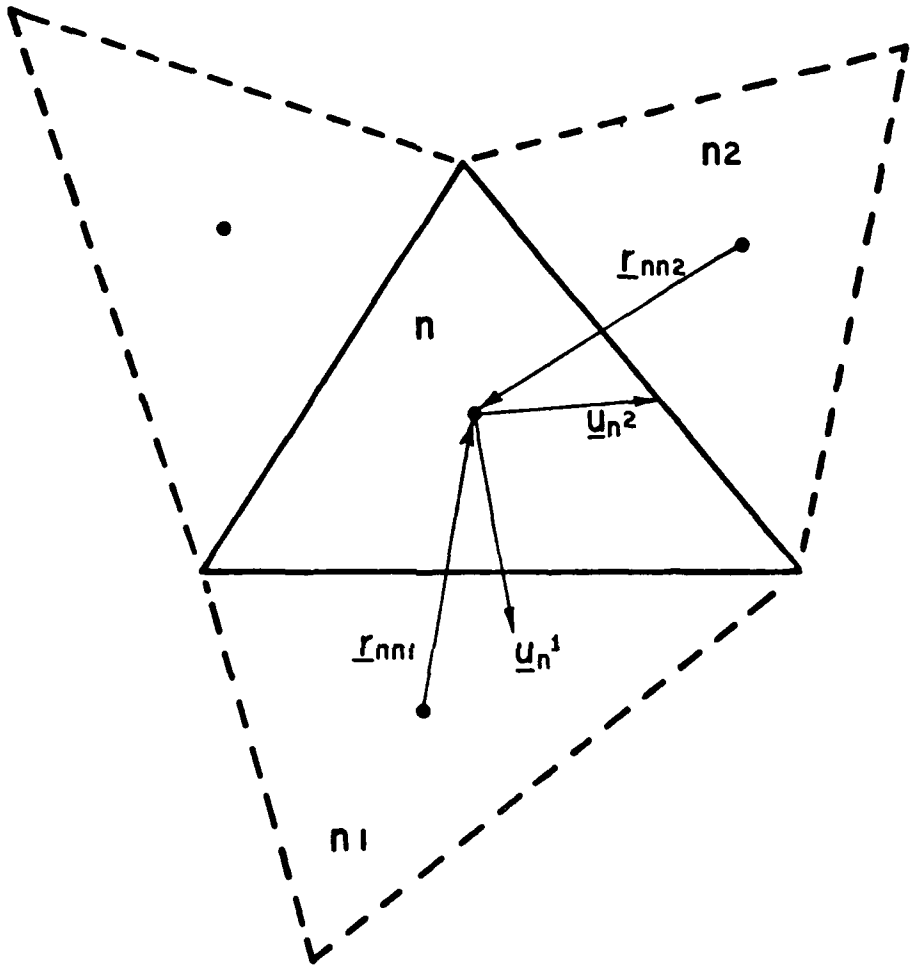

Figure 17. Geometry and basis vectors in the thin-shell surface-shell surface-patch algorithm.

SECTION V
CONCLUSIONS

Numerical testing for prolate spheroids, and finite circular and rectangular cylinders has demonstrated that the surface patch algorithms are efficient and accurate. These algorithms are also capable of handling sharp edges in rectangular box and finite cylinders. As compared with the wire-grid algorithms, the surface patch algorithm is more efficient with respect to computation speed and exhibits improved numerical accuracy, but has the disadvantage of unsymmetrical matrices. Improvements and limitations of this algorithm have also been discussed. Research efforts on the development of a thin-shell surface-patch algorithm is also presented. This thin-shell algorithm is being tested numerically for its accuracy and convergence.

SECTION VI

REFERENCES

1. F.K. Oshiro, "Source Distribution Technique for the Solution of General Electromagnetic Scattering Problems," Proc. First GISAT Symposium, Vol. 1, Part 1, Mitre Corporation, Bedford, MA., 1965.
2. F.K. Oshiro, K.M. Mitzner, and S.S. Locus, "Calculation of Radar Cross Sections," Technical Report AFAL-TR-70-21, Air Force Avionics Laboratory, Wright-Patterson AFB, Ohio, 1970.
3. N.C Albertsen, J.E. Hansen, and N.E. Jensen, "Computation of Radiation from Wire Antennas on Conducting Bodies," IEEE Trans. Ant. Prop., Vol. AP-22, No. 2, pp. 200-206, March 1974.
4. J.J.H. Wang, "Numerical Analysis of Three-Dimensional Arbitrarily-Shaped Conducting Scatterers by Trilateral Surface Cell Modeling," Radio Science, Vol. 13, No. 6, pp 947-952, November-December 1978.
5. D.K. Faddeer and V.N. Faddeeva, Computational Methods of Linear Algebra, W.H. Freeman and Co., San Francisco and London, pp 85-94, 1963.
6. J.H. Richmond, "Radiation and Scattering by Thin-Wire Structures in the Complex Frequency Domain," Report TR2902-10, ElectroScience Laboratory, Ohio State University, Columbus, Ohio, May 1974.
7. F.J. Deadrick and E.K. Miller, "A User's Manual for the Wire Antenna Modeling Program," Report UCID-30084, Lawrence Livermore Laboratory, University of California, Livermore, California, December 1973.
8. M.I. Sancer, S. Siegel, and A.D. Varvatsis, "Foundation of the Magnetic Field Integral Equation Code for the Calculation of Electromagnetic Pulse External Interaction with Aircraft," Report AFWL-TR-76-279, Air Force Weapons Laboratory, Kirkland AFB, New Mexico, April 1977.
9. L.L. Tsai, D.G. Dudley, and D.R. Wilton, "Electromagnetic Scattering by a Three-Dimensional Conducting Rectangular Box," Journal of Applied Physics, Vol. 45, No. 10, pp. 4393-4400, October 1974.
10. W.V.T. Rusch, J. Appel-Hansen, C.A. Klein, and R. Mittra, "Forward Scattering From Square Cylinders in the Resonance Region with Application to Aperture Blockage," IEEE Trans. Ant. Prop., Vol. AP-24, No. 2, pp 182-189, March 1976.
11. J.J.H. Wang, "Computer Modeling of Small Antennas on Aircraft," Proc. ECOM-ARO Workshop on Electrically Small Antennas, Fort Monmouth, New Jersey, pp. 147-151.
12. A.J. Poggio and E.K. Miller, "Integral Equation Solutions of Three-Dimensional Scattering Problems," Computer Techniques for Electromagnetics, edited by R. Mittra, Chapter 4, Pergamon, New York, 1973.
13. G.C. Copley, "Fundamental Results Concerning Integral Representations in Acoustic Radiation," J. Acoustic Soc. Amer., Vol. 44, No. 1, pp 28-32, January 1968.
14. H.A. Schenck, "Improved Integral Formulation for Acoustic Radiation Problems," J. Acoustic Soc. Amer., Vol. 44, No. 1, January 1968.

15. J. Boloney and W. Tabbara, "Numerical Aspects on Coupling between Complementary Boundary Value Problems," IEEE Trans. Ant. Prop., Vol. AP-21, No. 3, pp 356-363, May 1973.
16. J.R. Mantz and R.F. Harrington, "A Combined-Source Solution for Radiation and Scattering from a Perfectly Conducting Body," IEEE Trans. Ant. Prop., Vol. AP-27, No. 4, pp. 445-454, July 1979.
17. J.R. Mautz and R.F. Harrington, "H-Field, E-Field, and Combined Field Solutions for Conducting Bodies of Revolution," A.E.U. (Germany), Vol. 32, No. 4, pp. 157-164, April 1978.
18. C.M. Bulter and D.R. Wilton, "Analysis of Various Numerical Techniques Applied to Thin-Wire Scatterers," IEEE Trans. Ant. Prop., Vol. AP-23, No. 4, pp 534-540, July 1975.
19. J.J.H. Wang, "Software for Other Than Business-Oriented Computer Programs (Interim Software)," Contract No. F19628-78-C-0224, Deputy for Electronics Technology (RADC/EEA), Electronics Systems Command, Air Force Systems Command, Hanscom AFB, MA., June 1979.
20. D.L. Moffatt, "The Echo Area of a Perfectly Conducting Prolate Spheroid," IEEE Trans. Ant. Prop., Vol. AP-17, No. 3, pp 299-307, May 1969.
21. D.L. Moffatt and E.M. Kennaugh, "The Axial Echo Area of a Perfectly Conducting Prolate Spheroid," IEEE Trans. Ant. Prop., Vol. AP-13, pp 401-409, May 1965.
22. F.K. Oshiro, K.M. Mitzner, and R.G. Cross, "Scattering from Finite Cylinders by Source Distribution Technique," Proc of the GISAT II Symposium, Mitre Corp., Vol. II, Part I, 1967.
23. L.L. Tsai, D.G. Dudley, and D.R. Wilton, "Electromagnetic Scattering by a Three-Dimensional Conducting Rectangular Box," J. Applied Physics, Vol. 45, No. 10, pp 4393-4400, October 1974.
24. L.L. Tsai, "Radar Cross Section of a Simple Target: A Three-Dimensional Conducting Box," IEEE Trans. Ant. Prop., Vol. AP-25, No. 6, pp 882-884, November 1977.
25. R. Mittra, Y. Rahmat-Samii, D.V. Jamnejad, and W.A. Davis, "A New Look at the Thin-Plate Scattering Problems," Radio Science, Vol. 8, No. 10, pp 869-875, October 1973.
26. N.N. Wang, J.H. Richmond, and M.C. Gilbreath, "Sinusoidal Reaction Formulation for Radiation and Scattering from Conducting Surfaces," IEEE Trans. Ant. Prop., Vol. AP-23, No. 3, pp. 376-382, May 1975.
27. A. Mendelovicz, "A New Surface-Current Model for Metallic Scattering Surfaces," 1979 International Symposium Digest on Antennas and Propagation, Seattle, Washington, June 1979.
28. Y. Rahmat-Samii and R. Mittra, "Integral Equation Solution and RCS Computation of a Thin Rectangular Plate," IEEE Trans. Ant. Prop., Vol. AP-22, No. 4, pp 608-610, July 1974.
29. A. Sankar and T.C. Tong, "Current Computation on Complex Structures by Finite Element Method," Electronics Letters, Vol. 11, No. 22, pp 481-482, October 1975.

30. A.H. Stroud, Approximate Calculation of Multiple Integrals, Prentice Hall, Englewood Cliffs, New Jersey, 1966.
31. S.A. Schelkunoff and H.T. Friis, Antennas: Theory and Practice, John Wiley and Sons, New York, New York, 1952.
32. H.C. Pocklington, "Electrical Oscillations in Wire," Cambridge Phil. Soc. Proc., Vol. 9, pp 324-332, 1897.
33. R.H. Kyle, "Mutual Coupling between Log-Periodic Dipole Antennas," Ph.D. Dissertation, Syracuse University, Syracuse, New York, p. 23, 1968.
34. J.H. Richmond, "Digital Solutions of the Rigorous Equations for Scattering Problems," Proc. IEEE, Vol. 53, pp 796-804, 1965.
35. R.F. Harrington, "Field Computation by Moment Method," The MacMillan Company, New York, 1968.
36. G.A. Thiele, "Wire Antennas," Computer Techniques for Electromagnetics, R. Mittra - editor, Pergamon Press, New York, New York, 1973.

MISSION
of
Rome Air Development Center

RADC plans and executes research, development, test and selected acquisition programs in support of Command, Control Communications and Intelligence (C^3I) activities. Technical and engineering support within areas of technical competence is provided to ESD Program Offices (POs) and other ESD elements. The principal technical mission areas are communications, electromagnetic guidance and control, surveillance of ground and aerospace objects, intelligence data collection and handling, information system technology, ionospheric propagation, solid state sciences, microwave physics and electronic reliability, maintainability and compatibility.

Printed by
United States Air Force
Hanscom AFB, Mass. 01731